AD NUMBER

AD802157

NEW LIMITATION CHANGE

TO

Approved for public release, distribution unlimited

FROM

Distribution authorized to U.S. Gov't. agencies and their contractors; Administrative/Operational Use; FEB 1952. Other requests shall be referred to Ballistic Research Labs., Aberdeen Proving Ground, MD.

AUTHORITY

USAARDC ltr, 27 Oct 1980

ORDNANCE CORPS

BALLISTIC RESEARCH LABORATORIES

ABERDEEN PROVING GROUND, MD.

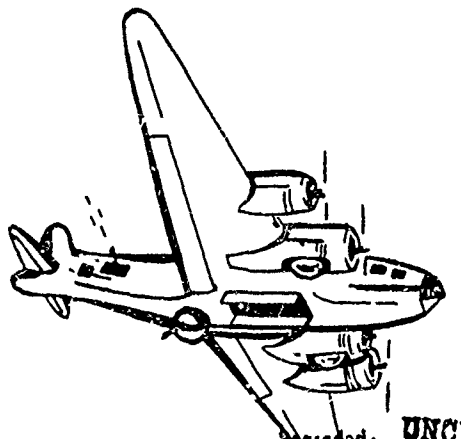

MEMORANDUM
REPORT No. 592

Body Nose Shapes for Obtaining High Static Stability

A. S. PLATOU

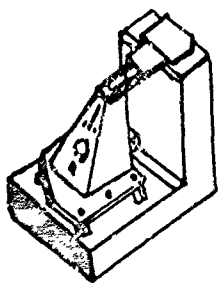

BALLISTIC RESEARCH LABORATORIES

MEMORANDUM REPORT NO. 592

February 1952

(9) Memorandum rept.,

(6) BODY NOSE SHAPES FOR OBTAINING HIGH STATIC STABILITY.

(10) A. S. Platou

(11) Feb 52

(12) 53 p.

(14) BRL-MR-592

(16)

Project No. ORD-TB3-0230A ~~of the Research and~~ Development Division, Ordnance Corps

ABERDEEN PROVING GROUND, MARYLAND

(050 750)

[redacted]

BALLISTIC RESEARCH LABORATORIES

MEMORANDUM REPORT NO. 592

ASPlatou/bts
Aberdeen Proving Ground, Md.
February 1952

BODY NOSE SHAPES FOR OBTAINING HIGH STATIC STABILITY

ABSTRACT

Wind tunnel tests at Ma = 1.7 have been run on various projectile nose shapes as part of a program to develop a short length 105mm spin stabilized shaped charge projectile. For satisfactory flight it is required that the projectile have a center of pressure much further aft than is required on a conventional shell. This is due to the rearward C.G. position of the shaped charge and to the small amount of spin which can be used without seriously decreasing the effectiveness of a shaped charge. The nose configurations chosen for test were those generating a minimum amount of lift, but still maintaining the required standoff distance for the shaped charge. Most of the configurations which accomplished this purpose have the conventional ogive replaced by a spike which produces a region of separated flow between the tip of the spike and the front of the main body. The results show that rearward center of pressure positions can be obtained by using these special configurations, however, the drag is higher than for a forward center of pressure configuration. With these configurations (which are 3.5 to 4 cal. long) it is possible to obtain centers of pressure which are up to 76% of the length aft of the nose compared to 48% of the length obtained with a cone cylinder of the same length.

[redacted]

INTRODUCTION

The criteria for satisfactory flight of an anti-tank shell involve accurate knowledge of the pitching moment about the C.G. and the drag. The pitching moment directly affects the missile stability and so is the prime result to be obtained from the wind tunnel tests. On the other hand the drag will affect the flight velocities and since it is desirable to maintain high velocities over the flight range it is desirable to have low drag.

An investigation of the aerodynamic characteristics of various nose configurations has been conducted as part of a development program on a 105mm short length shaped charge projectile. The investigation consisted of wind tunnel tests on these configurations at Ma = 1.7 to obtain accurate center of pressure, pitching moment, normal force, and drag data.

The requirements of the projectile are that it have a probable dispersion error of less than $\pm$ .5 mils at 1000 yards, be easily mass produced, and upon impact penetrate up to 12 inches of armour. The penetration requirement fixes the standoff distance and requires the projectile to have a low rate of spin since penetration decreases as spin increases.

The initial projectile configurations were to have a low rate of spin (1 rev. for 120 cal. forward travel) and were to have a stability factor at muzzle velocity (Ma 1.7) between 1-1/4 to 1-3/4. The S.F. limits were predicted from previous ballistic studies where the stability factor[1] is defined by:

$$S.F. = \frac{A^2}{4B}\left(\frac{\omega}{u}\right)^2 \frac{1}{\rho d^3 \frac{dK_m}{d\alpha}}$$

Inserting the values shown in the definition of symbols.

$$S.F. = \frac{47.5^2}{4 \cdot 122.7}\left(\frac{2}{120\,\frac{10.5}{2.54}}\right)^2 \frac{1}{.002378\left(\frac{10.5}{2.54}\right)^3 \frac{dK_m}{d\alpha}\frac{180}{\pi}}$$

---

[1] For additional information on the motion of a spinning projectile see BRL Report No. 446 by J. L. Kelley and E. J. McShane

then for S.F. = 1-1/4; $\frac{dK_m}{d\alpha} = +.00335$

and for S.F. = 1-3/4; $\frac{dK_m}{d\alpha} = +.00239$

Then assuming $\frac{dK_N}{d\alpha} \approx .02$ the required location of the center of pressure is .1 to .2 cal. ahead of the C.G.

Mr. R. H. Kent of this laboratory suggested a configuration of the E-20 type (see fig. 1). This configuration has a rearward C.G. (1.01 cal. from the base) and also has a rearward C.P. location, as can be seen from the data, due to the small amount of lift generated on the nose. However, the drag of this configuration is approximately 100% higher than that of an equivalent length cone cylinder and also there is a fairly violent flow oscillation at the nose.

No theoretical means are known for computing the flow on such a nose and therefore an empirical investigation was undertaken to obtain information on the following questions.

1. Is it possible to obtain a configuration having rearward C.P.'s, but lower drags than the E-20?

2. Is it possible to reduce or eliminate the flow oscillation observed on the E-20 nose by modifying the nose shape?

MODELS

The aerodynamic dimensions of the tested configurations are shown in figures 1, 2, 3, 4 and 5 with photographs of the model parts shown in figs. 6 and 7. These configurations were mounted on double pitching moment type strain gage beams which when used with a modified Brown potentiometer had the following accuracies.

Center of Pressure $\approx .05$ cal.

$K_N \approx .0005$

$k_m \approx .001$

The configurations were also adaptable to a normal strut and windshield so that lift and drag measurements could be obtained on the tunnel Tate Emory Balance. The lift and drag accuracy are $K_D \approx .001$ and $K_L \approx .002$.

DEFINITION OF SYMBOLS

Air Characteristics

a = speed of sound

U = velocity of air or projectile

P_o = stagnation pressure

P_{TS} = test section static pressure

T_o = stagnation temperature

q = dynamic pressure = $1/2\ \rho\ U^2 = \frac{\gamma}{2} P_{TS}\ Ma^2$

ρ = density of air

μ = viscosity of air

γ = ratio of specific heats = $\frac{C_p}{C_v}$

S.H. = specific humidity

Miscellaneous

Ma = Mach Number

Re = Reynolds No. = $\frac{\rho . u\ d}{\mu}$

C.P. = Center of pressure

$$S.F. = \frac{A^2\ \omega^2}{4Bu^2\ \rho d^3\ \frac{dK_m}{d\alpha}}$$

A = moment of inertia of projectile about axis of symmetry = $4.75\ in^2$ #for the E-20

B = moment of inertia of projectile about axis through the center of gravity and perpendicular to the axis of symmetry = $122.7\ in^2$ #for the E-20

Model Characteristics

d_B = max body dia.

d_b = base dia.

S_b = base area

C.G. = center of gravity

Forces, Moments and Pressures

D_i = indicated drag

D_b = base drag

D_F = fore drag

N = normal force

$m_{C.G.}$ = pitching moment about C.G.

P_b = model base pressure

Angles

α = angle of attack

ω = angular velocity of projectile $\left(\frac{\omega}{u} = \frac{2}{120 \times \frac{10.5}{2.54}} = .01265 \frac{\text{rad}}{\text{in/sec}} \right)$

Force and Moment Coefficient

K_{D_i} = indicated drag coefficient = $\frac{D_i}{\rho u^2 d_B^2}$

K_{D_b} = base drag coefficient = $\frac{(P_{TS} - P_b) S_b}{\rho u^2 d_B^2}$

K_{D_F} = fore drag coefficient = $K_{D_i} - K_{D_b}$

K_L = lift coefficient = $\frac{L}{\rho u^2 d_B^2}$

K_N = normal force coefficient = $\frac{N}{\rho u^2 d_B^2}$

$$K_{m_{CG}} = \text{pitching moment coefficient about C.G.} = \frac{m_{C.G.}}{\rho u^2 d_B^3}$$

$$C.P._{CG} = C.P. - C.G. \text{ dist. in cal.} = \frac{K_{m_{C.G.}}}{K_N}\left(\text{near } \alpha = 0^\circ \; C.P. = \frac{\frac{dK_m}{d\alpha}}{\frac{dK_N}{d\alpha}}\right)$$

TEST PROCEDURE AND DATA REDUCTION

The following tunnel conditions were used during these tests.

$M_\infty = 1.72$

$P_o = 96$ cm Hg abs.

$q = 7.563$ P.S.I.

$Re = .405 \times 10^6$ per inch

Dew Point $< -30^\circ F$

$T_o \approx 100^\circ F$

All of the models were mounted on the tunnel centerline at zero angle of attack and could be rotated through angles of attack between $\pm 10^\circ$. Each test consisted of obtaining force and moment data at indicated angles of attack between $\pm 10^\circ$. Also schlieren pictures were taken at $\alpha = 0, \pm 6$, and $\pm 10^\circ$ during each test and high speed schlieren movies were taken in order to study the flow oscillations occurring on some of the configurations. Additional tests were run on each configuration using the Tate Emory Balance system in order to obtain drag and lift data.

The data were reduced to coefficient form using the equations shown in the definition of symbols. All data have been corrected for strut deflection and have been forced through zero in an attempt to correct for variation of tunnel flow inclination.

RESULTS AND DISCUSSION

E-20 Configuration

The data on the original nose shape (E-20) are shown in figs. 12 and 13. This configuration has centers of pressure at angles

of attack up to 5° which are in approximately the desired position with respect to the C.G. and approximately 1.1 cal. aft of the cone cylinder (E-23C) centers of pressure. The desired C.P. to C.G. distance of .2 cal could be obtained from this configuration by varying the projectile weight distribution.

It can also be seen from figs. 26 and 27 that a conical separated region occurs in front of the main body (1 cal. dia.). Therefore, the blunt surface of the body is subject to approximately the conical surface pressure instead of the approximate total head pressure as would be the case of a blunt cylinder minus the spike. Since a conical surface pressure is much less than the corresponding total head pressure the drag of the spiked body will be much less than the drag of the blunt cylinder minus the spike. The drag and other aerodynamic data for a blunt cylinder E-23Q are compared with the E-20 and cone cylinder E-23C data in figs. 12-13.

Tests on the E-20 configuration over a Reynolds No. range from $.59 \times 10^6$ to $.13 \times 10^6$ per inch indicated no change in pitching moment, normal force or C.P. location.

During the testing of the E-20 flow oscillations on the nose were observed. Figs. 26 and 27 are two schlieren photos of the E-20 taken at different times. The frequency of the oscillation is 1000 to 1500 C.P.S. as estimated from high speed schlieren films and appears to be similar to the oscillation occurring on a ramjet operating above maximum compression ratio. However, it is believed that the oscillation will not affect the flight characteristics seriously since the frequency is much higher than any other flight frequencies. Some of the other frequencies are 1) rate of nutation 10.3 rev/sec at Ma = 1.42 to 20.6 rev/sec at Ma = 1.98, 2) rate of precession 1.3 rev/sec at Ma = 1.42 to 2.4 rev/sec at Ma = 1.98. These are representative values determined from free flight tests of the T-138 E-20 configuration.

However, energy must be dissipated in the oscillation and as a result the drag of the missile increased. Therefore, if the oscillation can be reduced or eliminated the drag should be reduced.

Data for the various configurations tested are presented in figs. 12 to 24 and in order to compare the effectiveness of these configurations, graphs of drag vs pitching moment and drag vs center of pressure at constant angles of attack are presented in figs. 8 to 11. From these graphs the configurations having the least drag of those tested for any particular pitching moment or center of pressure can be easily determined. The points representing the various configurations having minimum drag have been connected with a solid line thereby establishing a minimum drag curve for

the tested configurations. It is possible that other nose configurations may have lower drags than those tested and the minimum drag curve established in this report can be used to compare other nose configurations with the reported configurations. The comparison can be made at any desired angle of attack for which data are available and in this case 0° and 5° angles of attack were chosen.

Conical Screen Nose Configurations

To eliminate the oscillation observed on the E-20, configurations were tested in which screens formed a conical surface between the spike tip and the main body (see figs. 6 & 7). The function of the screen is to provide a damping mechanism for the oscillation without generating a large amount of lift. It can reasonably be surmised that the amount of generated lift is a function of the screen solidity ratio and the most desirable screen is one which prevents the oscillation and also produces the minimum amount of lift.

In an attempt to determine the best screen solidity three configurations (E-23J, K & N having 56%, 31% and 19% solidity ratios respectively) were tested. High speed schlieren movies show that the oscillation is eliminated on all three configurations thereby indicating that the best solidity ratio is less than 19%. Configurations having further reduction in screen solidity cannot be built from standard flat screening for noticeable asymmetries in the conical screen and in the aerodynamic data would result. Such asymmetries are appearing in the E-23N configuration as seen in figs. 7 and 15.

Besides eliminating the oscillations the three configurations have centers of pressure .2 to .5 cal. forward of the E-20 configurations and approximately .6 to .9 cal. aft of the cone cylinder configuration E-23C. These configurations are on the minimum drag curve (figs. 8, 9, 10 and 11) and have approximately 25% less drag than the E-20 configuration.

At angles of attack there will be a flow through the screen from the windward side to the leeward side. In order to keep the lift to a minimum the material inside the screen must be kept to a minimum so that the air flow through the screen is a maximum. Since body volume in this region will generate a lift of its own it should be as poor a lifting surface as possible. The generation of such lift is indicated by the results obtained on configurations E-23, E & G in figures 14 and 15.

Truncated Cone Configurations

A second series of tests on truncated cone noses produced similar aerodynamic results. These shapes are probably more

practical than the screen nose from a production view point. The best of these configurations (E-23B, L and M) lie on the minimum drag curve and have C.P. positions .4 to .7 cal. forward of the E-20 configuration and .4 to .7 cal. aft of the cone cylinder E-23C. The oscillation amplitude is considerably reduced as shown by high speed schlieren pictures and the drag is also reduced compared to the E-20 configuration. The three configurations differ in the amount of truncation and the test results show that the center of pressure moves forward and the drag decreases as the amount of truncation is increased.

Another configuration which can be included in the truncated cone series is the truncated conoid (E-23H). This proved undesirable in that the center of pressure is too far forward and the drag is too high. (See figs. 18 & 19.) The drag increase over E-23F is probably due to the compression over the curved surface as can be seen in the schlieren photos, figs. 45 and 47.

Tests with and without the 15° nose tip cone (E-23B and E-23F) indicate that the nose cone decreased the drag ($\Delta K_D = .014$) and moves the C.P. forward a small amount. A calculation assuming the drag of the blunt tip to be 92% of the stagnation pressure behind a normal shock multiplied by the tip area and that the cone tip drag is equal to the calculated cone surface pressure multiplied by the base area shows the drag difference between the conical tip and the blunt tip to be the same as that obtained experimentally on the E-23B and E-23F. However, the drag difference between the E-20 and E-23F is only .005 and this discrepancy is not fully explained. In view of the large oscillations present it is quite possible that the change in tip shape has a larger effect on the average pressure on the front of the E-20 body than on the E-23F.

Other changes in the nose tip configuration (E-22, 23, 23A) yield high drag values and consequently placed them above the minimum drag curve.

A comparison (figs. 15 & 17) of the center of pressure travel with angle of attack of the three types of configurations (E-20, screen nose, and truncated cone nose) shows that the E-20 has the least C.P. travel +.05 cal. up to $\alpha = 8°$. The screen nose C.P.'s moves forward .1 to .25 cal. depending on the screen mesh and the truncated cone C.P.'s move rearward .1 to .15 cal. depending on the degree of truncation.

A study of the separated region existing on the noses of several of these configurations indicates that the surface of this region appears to approach asymptotically a conical surface lined up with the free stream direction regardless of the angle of attack of the

missile. Angle measurements (at various angles of attack) made as far downstream as possible on the separation surface for configurations E-20, E-23B, E-23L, E-23M and E-23A show that the maximum angle between the centerline of the separation cone and the direction of the free stream is 2°, which is within the accuracy of measurement. This behavior leads one to believe that the separated region, except near the front of the cylinder, is approximately a constant pressure region.

Extended Body Configurations

The aerodynamic characteristics of extended body (1/2 and 1 caliber extensions) configurations were investigated on the E-20, E-23K and E-23M; the objective was to determine whether additional lift could be obtained by adding additional body. The data (figs. 22 to 24) show either no C.P. motion or a slight forward motion of the C.P. thereby indicating that the lift distribution reaches zero or minus values at or before the 2 caliber length is reached. Similar results are obtained using a conventional ogive nose as shown by various body alone tests.

Pine Cone Configuration

A pine cone nose configuration (E-23D), which was adopted from a German configuration tested during World War II, is on the minimum drag curve. However, its center of pressure is only .2 cal. aft of the cone cylinder (E-23C) thereby indicating that it is inefficient as a lift destroying mechanism. The aerodynamic data are presented in figs. 18 and 19.

Dual Flow Pattern Configurations

On all of the spiked nose configurations mentioned previously, the flow separates from the spike at the spike tip. However, on configurations E-21, E-23I, and E-23P it is possible to obtain two flow patterns, one in which the flow separates from the nose tip (called the 1st flow pattern) and one in which the flow separates from the spike a considerable distance aft of the tip (called the 2nd flow pattern), figs. 32, 33, 48, 63 and 64.

The first flow pattern is obtained when the tunnel flow is first established and with two of the three configurations tested it is usually necessary to change angle of attack before the second flow occurs. The angles of attack at which the flow trips from one condition to the other is not consistent for all configurations and therefore, no general statement concerning the conditions for tripping can be made. Below is the information observed on each of the three dual flow configurations tested.

E-21

1st flow pattern occurs when tunnel flow is established and usually maintains itself between $\alpha \approx \pm 5$, however, at infrequent intervals the 2nd flow pattern will occur at $\alpha = 0^{\circ}$ shortly after the tunnel flow is established. Once the 2nd flow pattern is established it usually persists regardless of the angle of attack. At infrequent intervals between $\alpha = 6^{\circ}$ to 8° the flow pattern trips back and forth.

E-23I

1st flow pattern occurs when tunnel flow is established and maintains itself between $\alpha \approx \pm 2^{\circ}$. Once the 2nd flow pattern is established it persists regardless of angle of attack.

E-23P

1st flow pattern persists at all angles of attack except low angles ($\alpha \approx \pm 1^{\circ}$) where flow pattern trips back and forth at irregular intervals.

The existence of this phenomenon means that some spiked nose configurations are unable to maintain completely separated flow at all times and that the existence of dual flow is a function of the nose geometry, among other things. The exact conditions for avoiding this phenomenon are unknown and at present it is necessary to conduct wind tunnel tests to determine if it exists on a particular configuration.

Force and moment tests show that the drag, pitching moment, and center of pressure are different for the two flow patterns while no change can be detected in the normal force and lift. The first flow pattern has a lower drag and a more forward center of pressure, however, the E-21 second flow C.P.'s move forward considerably at high angles of attack.

This phenomenon may be due to wind tunnel test conditions which are not present during free flight (ex., the wind tunnel starting shock may be a sufficiently large pressure disturbance to establish the first flow pattern). Free flight tests are being planned to determine its existence or non-existence. If the phenomenon does occur in free flight the projectile flight would be unsatisfactory due to the large shifts in center of pressure compared to the desired C.P.-C.G. distance. If only the second flow pattern occurs then configurations such as the E-21 etc. may be desirable due to the rearward C.P.'s obtained at small angles of attack.

Larger Standoff Configurations

A screen nose configuration (E-23 "0") having a standoff distance about the same as the E-21 and greater than the other configurations was also tested. From data (figs. 14 and 15) it is seen that its performance is similar to that of a solid cone in that the center of pressure moves forward and the drag decreases. The drag decrease between E-23 "0" and E-23K is .015 while for equivalent solid cones the drag decrease is computed to be .047. This configuration lies slightly below the minimum drag curve and indicates the curve for longer noses should lie slightly below the ones shown. The screen also prevents the occurence of the second flow pattern found on the E-21.

One additional test on the configuration E-1 was requested and the data obtained are plotted in figs. 20 and 21. This configuration was one of the initial missiles fired by the Aerodynamic Range during the early part of this development program.

Ma = 1.3 Tests

Tests at Ma = 1.3 have been run on the E-20, E-23K and E-23M but due to malfunctioning of the instrumentation the data are not of sufficient accuracy to present at this time. However, center of pressure data have been obtained in the Aerodynamic Range on the E-20 and are presented in fig. 25. These data show a very significant Mach No. effect. The C.P. moves forward as the Ma decreases to Ma $\approx$ 1.2 and then moves rearward as the Ma decreases through 1.0.

CONCLUSIONS

1. A minimum drag vs C.P. or moment curve has been established at Ma = 1.7 for the family of configurations tested. This curve determines the configurations of those tested having minimum drag for any desired pitching moment or center of pressure position. The configuration lying on or near this curve are the conical, the pine cone, the screened, the truncated cone and the blunt spiked (E-20) noses.

2. The maximum rearward C.P. position obtainable with a satisfactory configuration was approximately 76% of the length aft of the nose. This was obtained with the blunt spiked configuration E-20 while the most forward C.P. position of 48% was obtained with the full cone configuration E-23C. However, the rearward C.P. configurations are accompanied by a drag increase. Screen and truncated cone nose configurations give C.P.'s slightly

forward of the E-20 C.P., and have 25% less drag than the E-20.

3. All of the spiked nose configurations exhibit a flow oscillation which appears similar to that observed on a ram jet operating at maximum compression ratio. Truncated cones reduce the oscillation amplitude and screen noses eliminate the oscillation.

4. Two flow patterns, which trip back and forth at irregular intervals, are obtained on several of the extended spiked nose configurations. These flows establish different aerodynamic force characteristics on the missile and may produce erratic motions of the missile in free flight. Free flight tests on a dual flow configuration have not yet been made.

5. The minimum amount of screening required to stop the flow oscillations on the spiked noses is less than 19% solidity. The screens also prevent the dual flow pattern.

6. These noses are adaptable to other missiles, particularly fin stabilized missiles where the overall length has to be kept as small as possible. Tests of the E-20 and E-23K noses on a finned configuration indicate that a missile with fins will have much better stability than the same configuration with an ogive nose. A second report covering the effect of these noses on fins will be published shortly.

A. S. Platou

A. S. Platou

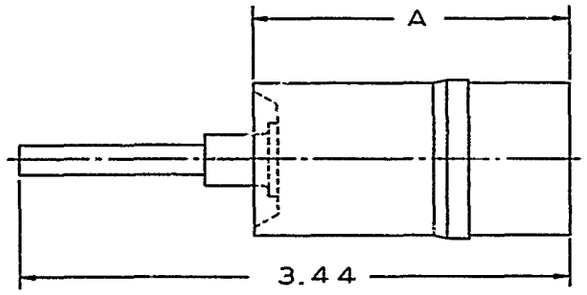

E-20 A = 1.98
E-20a A = 2.48
E-20b A = 2.98

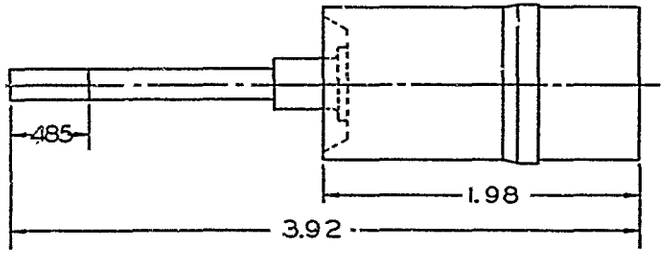

E-21

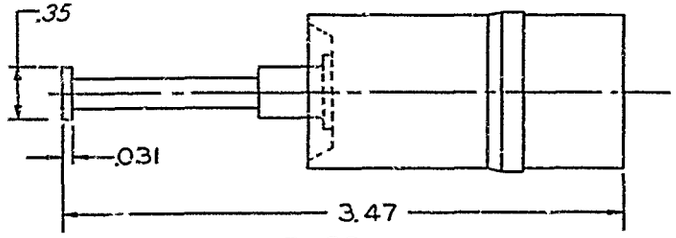

E-22

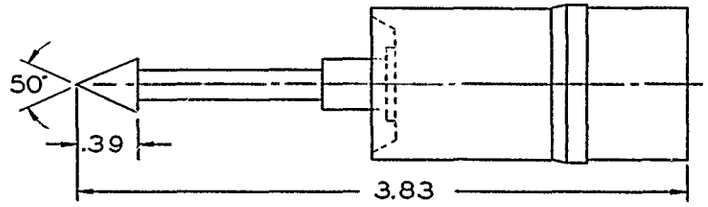

E-23

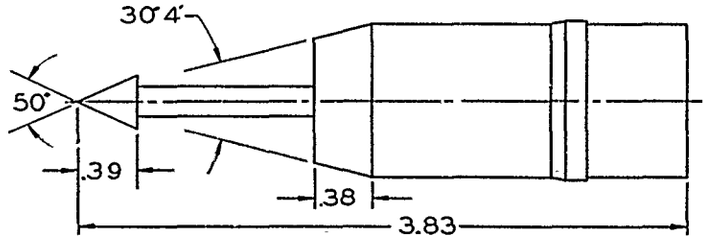

E-23A

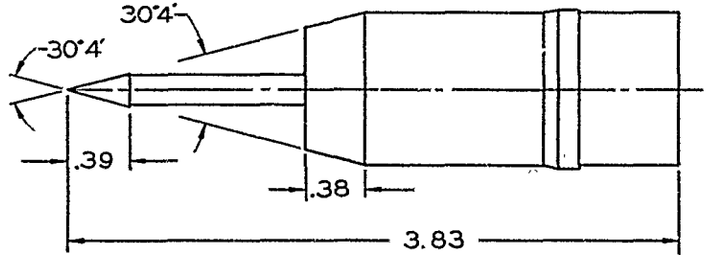

E-23B

CENTER OF GRAVITY FOR ALL CONFIGURATIONS = 1.01 CALIBERS FROM BASE.
ALL DIMENSIONS IN CALIBERS - 1 CALIBER = 2.50 INCHES.

FIG 1

105 m/m, T-138 CONFIGURATIONS

SUPERSONIC WIND TUNNELS | 4 JUNE 51

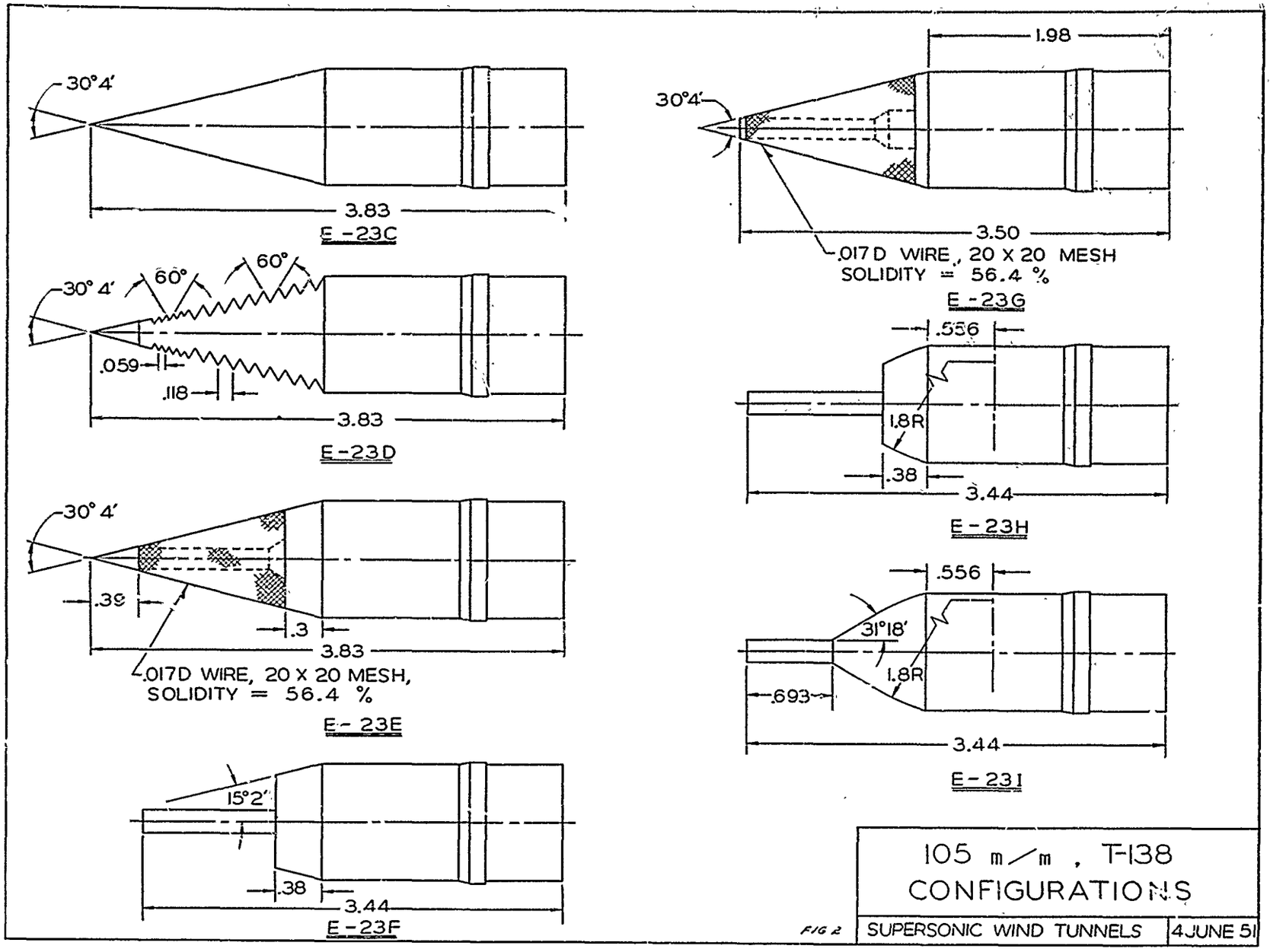
30°4'
3.83
E-23C
30°4'
60°
60°
.059
.118
3.83
E-23D
30°4'
.39
.3
3.83
.017D WIRE, 20 X 20 MESH,
SOLIDITY = 56.4 %
E-23E
15°2'
.38
3.44
E-23F
1.98
30°4'
3.50
.017D WIRE, 20 X 20 MESH
SOLIDITY = 56.4 %
E-23G
.556
1.8R
.38
3.44
E-23H
.556
31°18'
1.8R
.693
3.44
E-23I
105 m/m, T-138
CONFIGURATIONS
FIG 2
SUPERSONIC WIND TUNNELS
4 JUNE 51

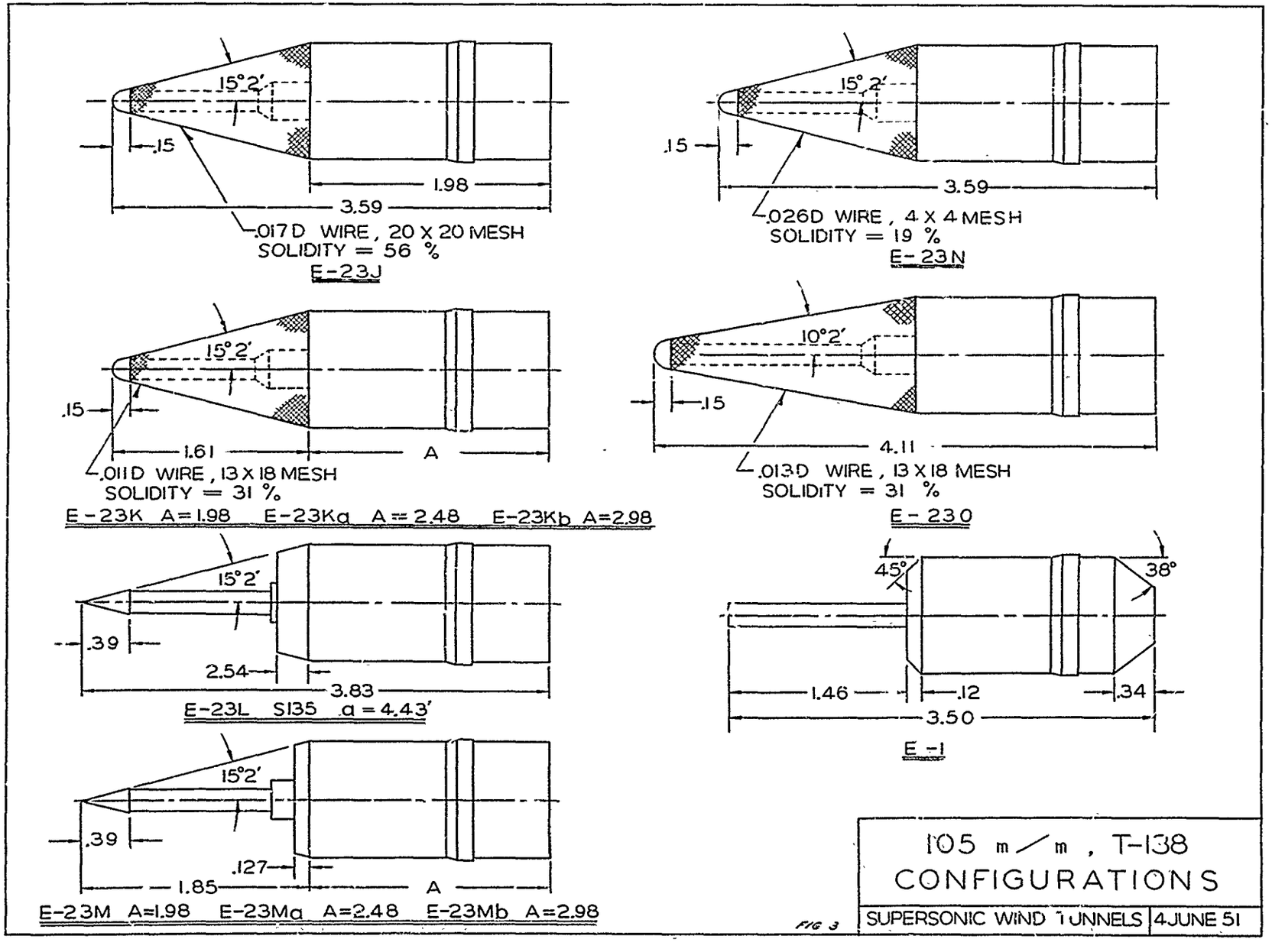

FIG 3

105 m/m, T-138
CONFIGURATIONS

SUPERSONIC WIND TUNNELS | 4 JUNE 51

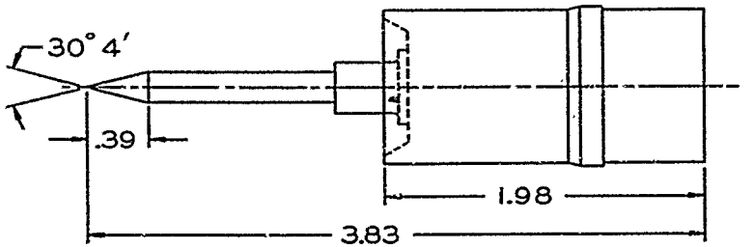

E - 23 P

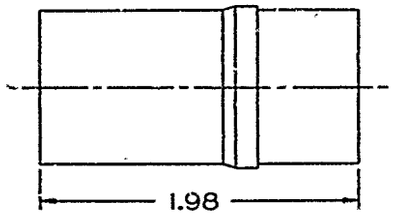

E- 23 Q

ALL DIMENSIONS IN CALIBERS - 1 CALIBER = 2.50 INCHES

FIG 4

105 m/m , T-138
CONFIGURATIONS

SUPERSONIC WIND TUNNELS | 17 SEPT 51

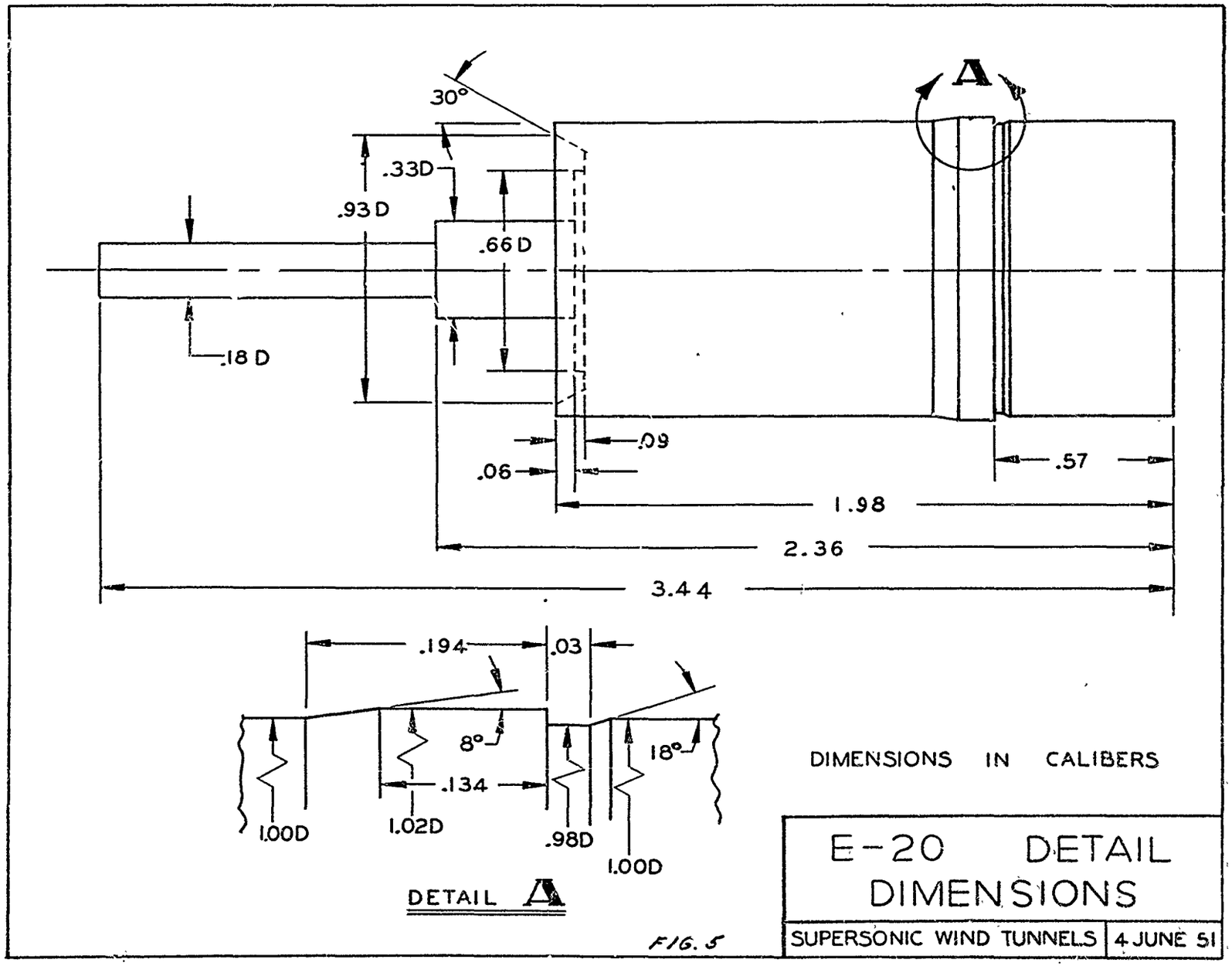
30°
.33D
.93 D
.66 D
.18 D
A
.09
.06
.57
1.98
2.36
3.44
.194
.03
8°
18°
.134
1.00D
1.02D
.98D
1.00D
DETAIL A
DIMENSIONS IN CALIBERS
E-20 DETAIL DIMENSIONS
SUPERSONIC WIND TUNNELS
4 JUNE 51

FIG. 5

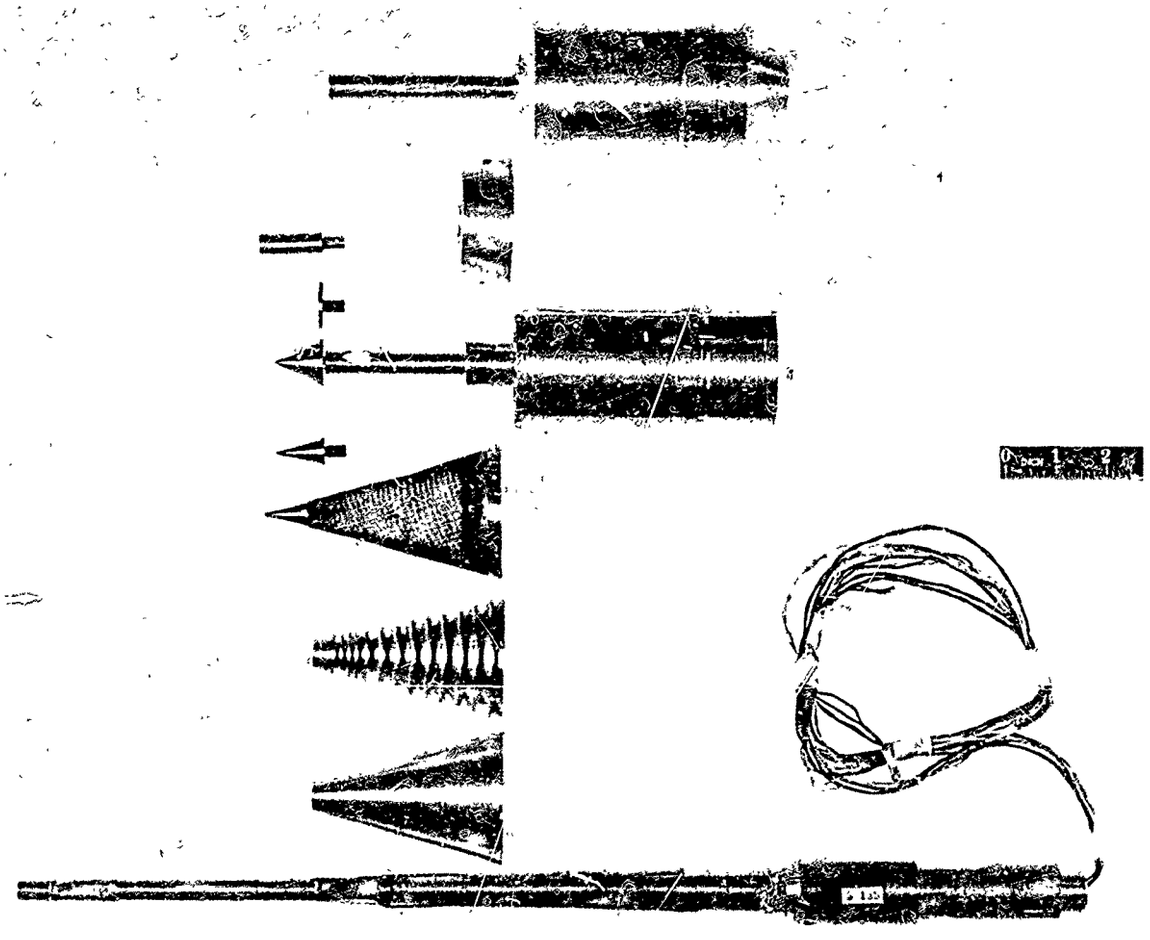

FIG. 6. MPS 714, 105mm Shell, T138.

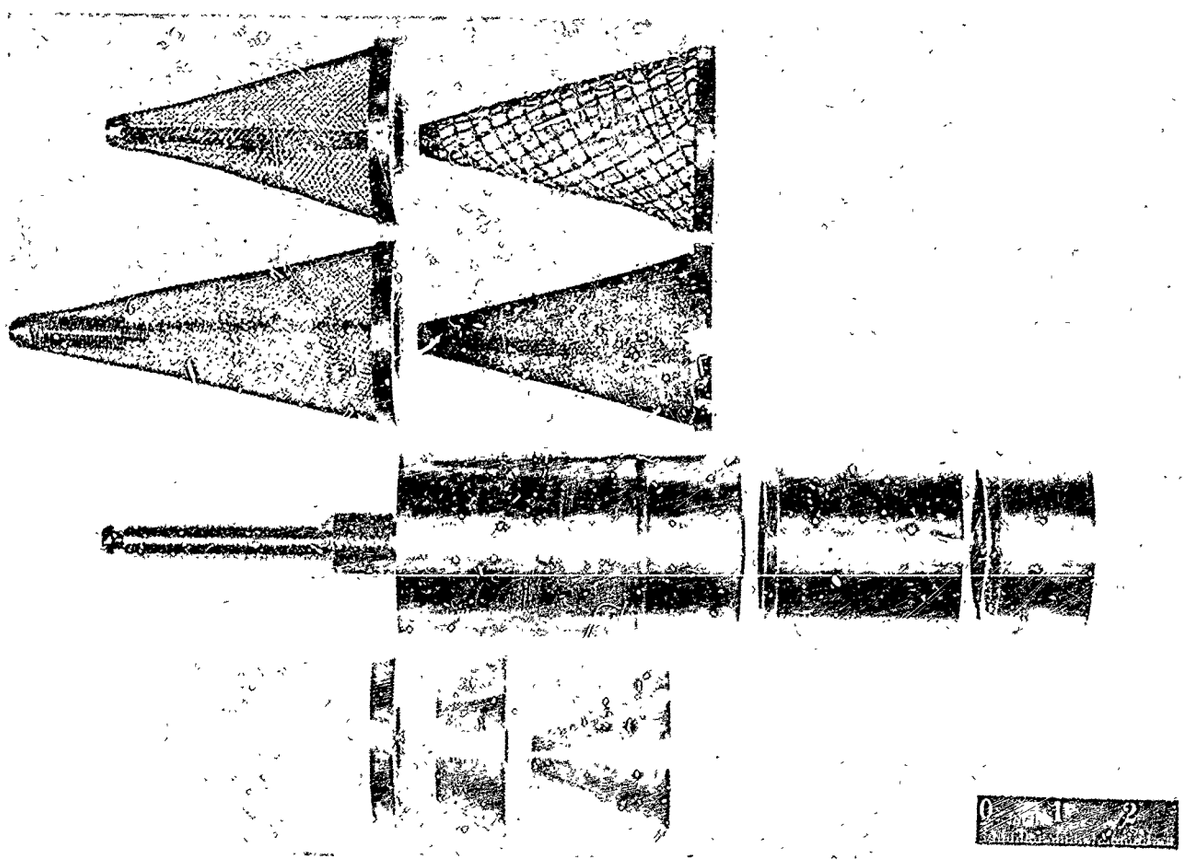

FIG. 7. MPS 714, 105mm Shell, T138.

Kop , Force Drag Coefficient
.25
.20
.15
.10
.05
0
-.005
0
.005
.010
.015
.020
.025
dKm²/dd
α=0°
Re = 4.2 X 10⁶ per Inch
M∞ = .172
* Dual Flow Configurations
1st Flow
2nd Flow

Fig 2

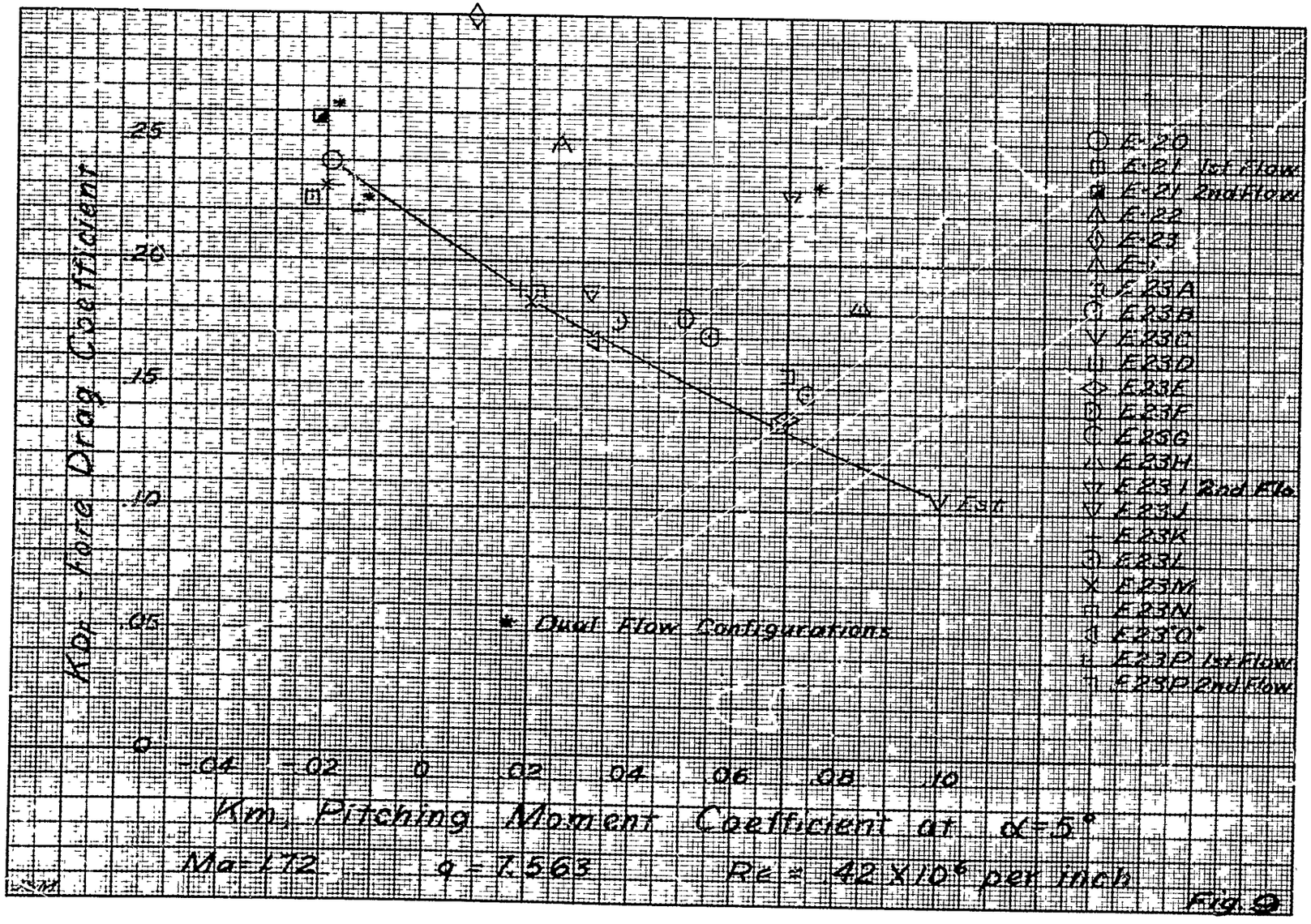
Kor Total Drag Coefficient
.25
.20
.15
.10
.05
0
-.04
-.02
0
.02
.04
.06
.08
.10
* Dual Flow Configurations
E-20
E-21 1st Flow
E-21 2nd Flow
E-22
E-23
E-
E 23A
E 23B
E 23C
E 23D
E 23E
E 23F
E 23G
E 23H
E 23 I 2nd Flo
E 23J
E 23K
E 23L
E 23M
E 23N
E 23O
E 23P 1st Flow
E 23P 2nd Flow
Km Pitching Moment Coefficient at α=5°
Ma=1.72 q=1.563 Re = 42 x 10⁶ per inch
Fig 9

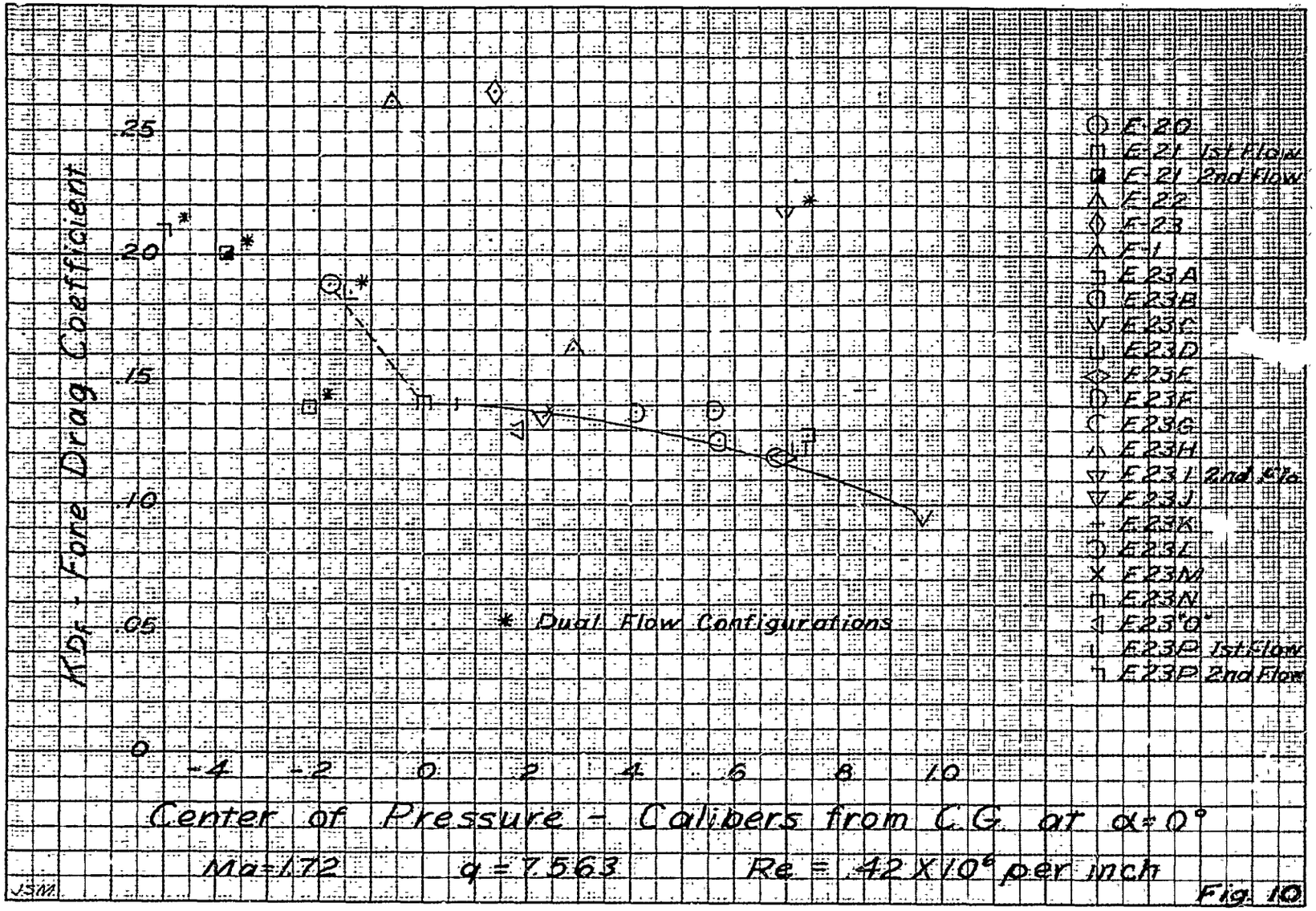

Center of Pressure - Calibers from C.G. at $\alpha = 0°$

$Ma = 1.72$ $q = 7563$ $Re = .42 \times 10^6$ per inch

JSM

Fig. 10

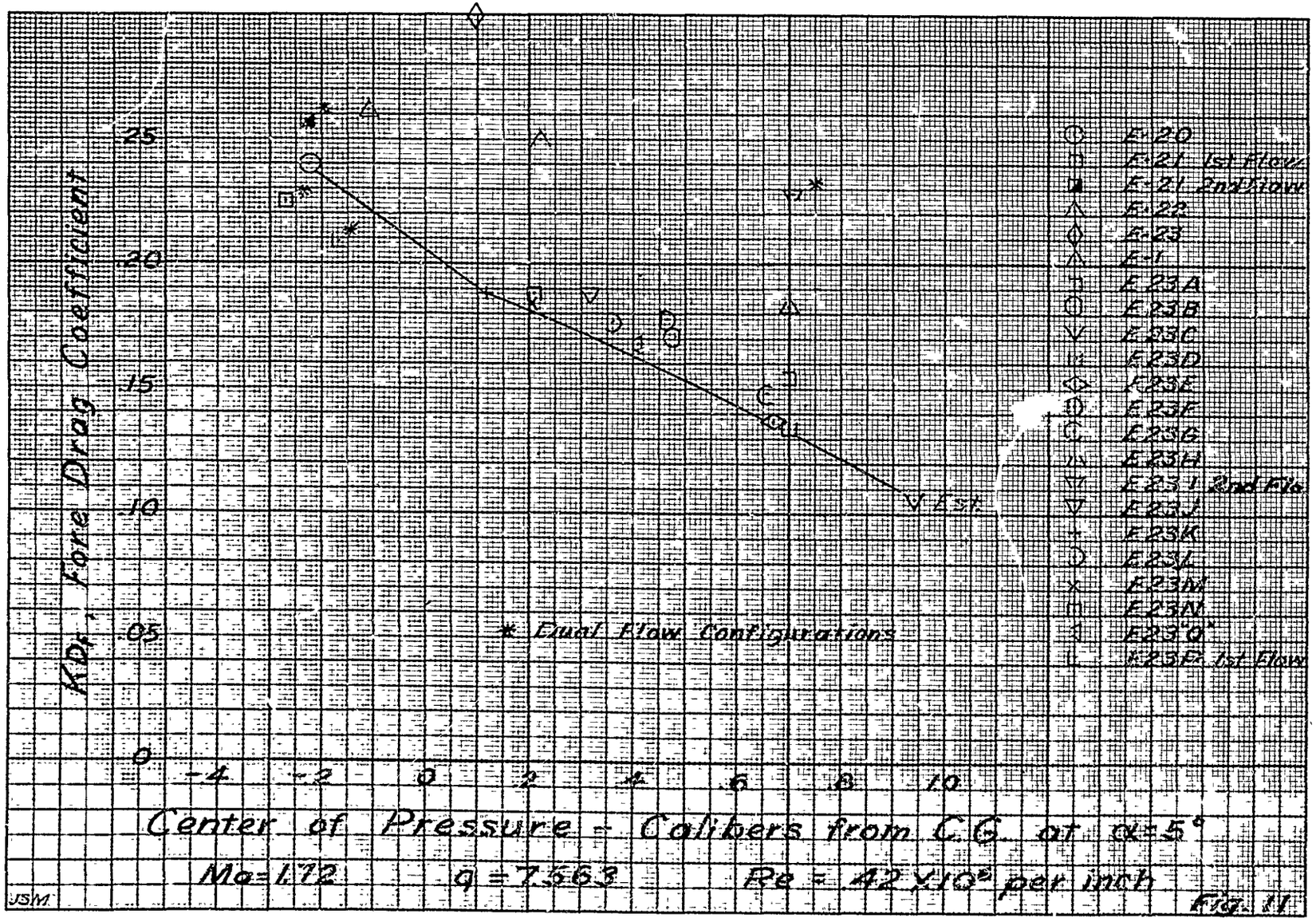
KDf, Fore Drag Coefficient
.25
.20
.15
.10
.05
0
-4
-2
0
2
4
6
8
10
Est
* Equal Flow Configurations
F-20
F-21 1st Flow
F-21 2nd Flow
F-22
F-23
F-1
F-23A
F-23B
F-23C
F-23D
F-23E
F-23F
F-23G
F-23H
F-23 I 2nd Flo
F-23J
F-23K
F-23L
F-23M
F-23N
F-23O
F-23P 1st Flow
Center of Pressure - Calibers from C.G. at α=5°
Ma=1.72
q=7563
Re = .42 X 10⁶ per inch
JSM
Fig. 11

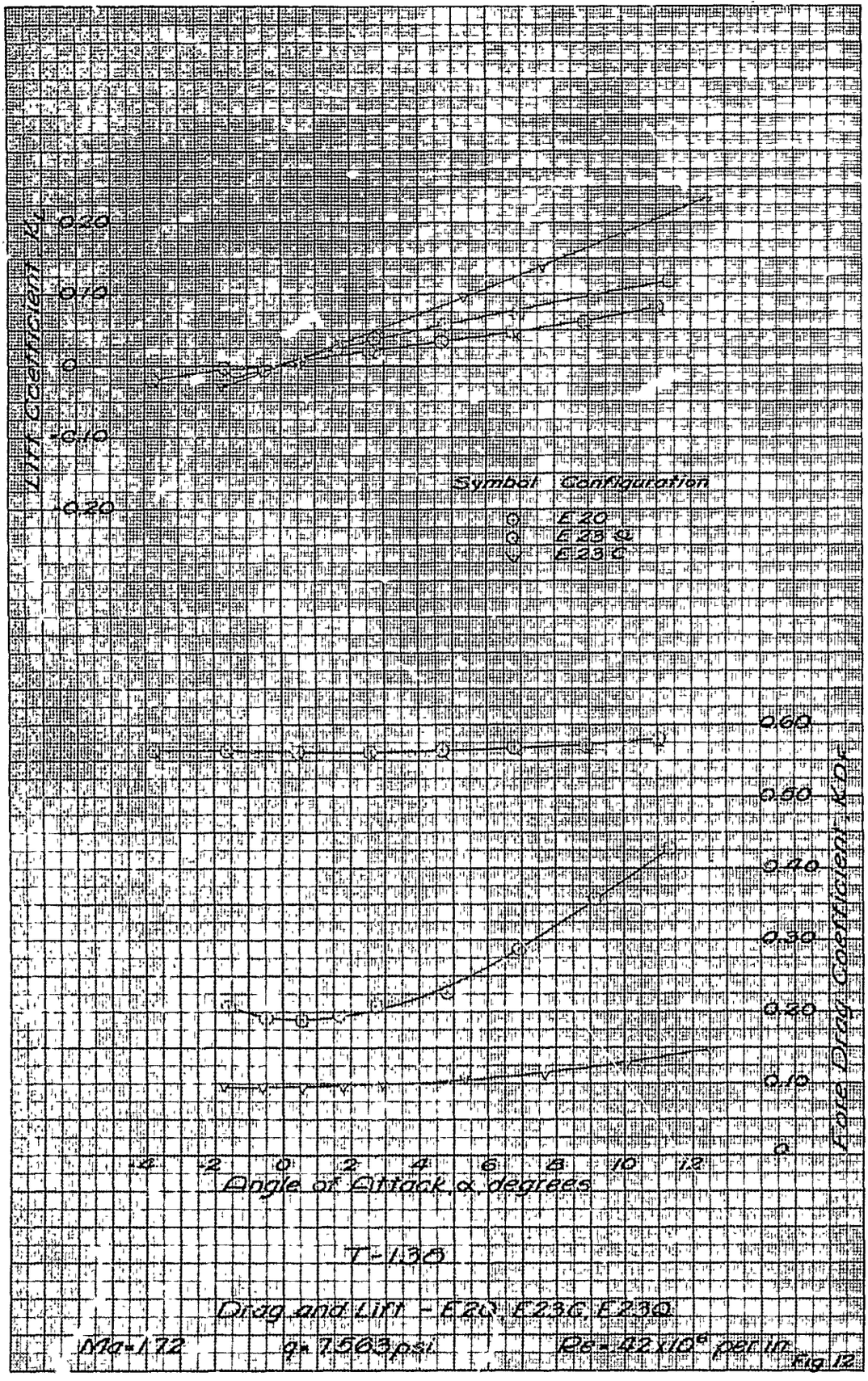
Lift coefficient C_L
-0.20
-0.10
0
0.10
0.20
Symbol Configuration
E 20
E 23 C
E 23 C
0.60
0.50
0.40
0.30
0.20
0.10
0
Note Drag coefficient C_D
-4
-2
0
2
4
6
8
10
12
Angle of Attack α degrees
T-1306
Drag and Lift - E20, E23C, E23D
M_a=1.72
q=7563 psi
R_e=.42x10^6 per in.
Fig 12

T-1363

Normal Force, Pitching Moment and Center of Pressure Data

E20 E23C E23Q

M_a=1.72 q=7,563 psf R_e=.42x10⁶ per in. Fig 15

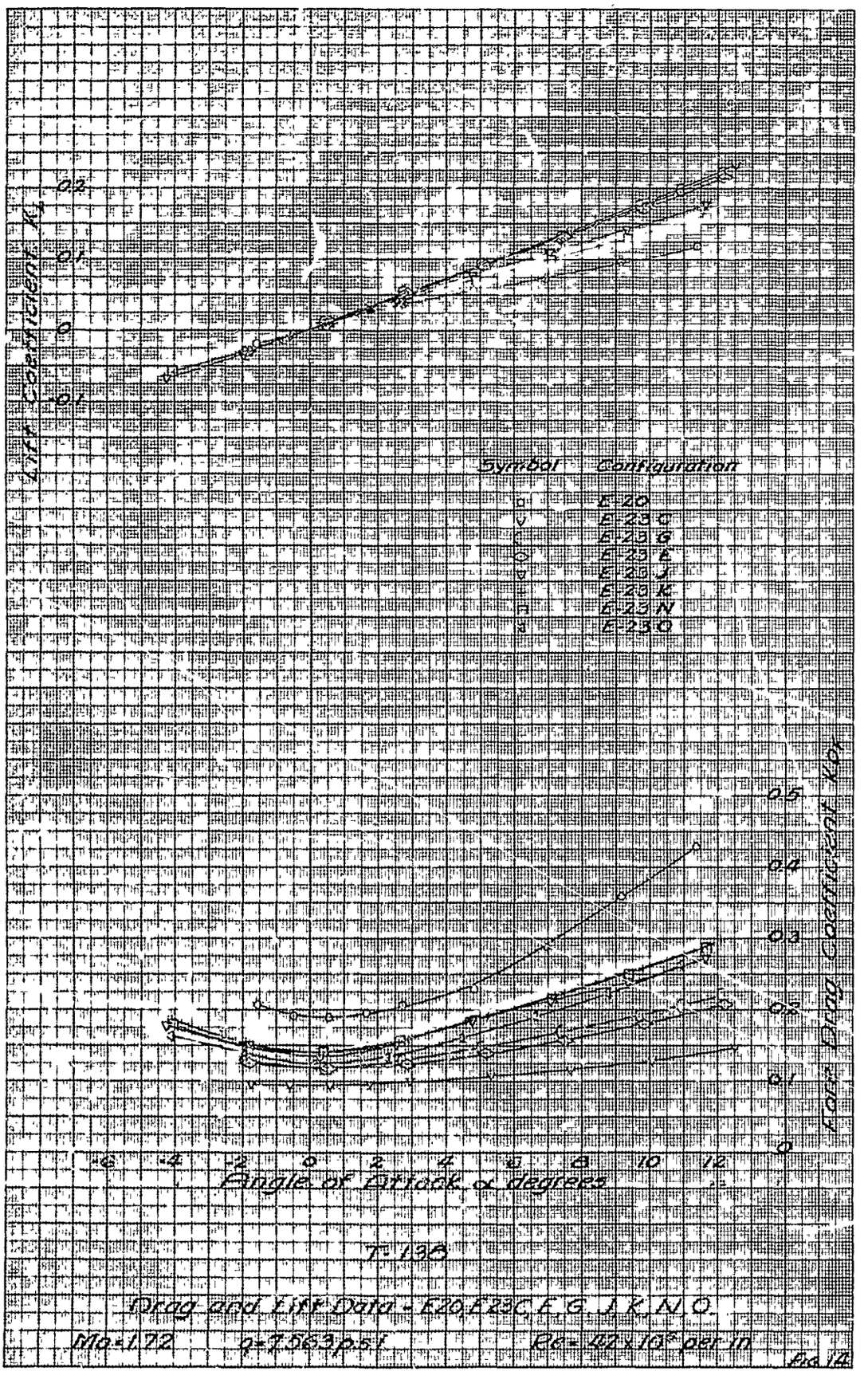
Lift Coefficient, C_L
Drag Coefficient, C_D
Symbol Configuration
E 20
E 23 C
E 23 G
E 23 E
E 23 J
E 23 K
E 23 N
E 23 O
Angle of Attack, α degrees
T: 136
Drag and Lift Data - E20 E23C E G J K N O
Ma=1.72 p=7563 p.s.f. Re = 42 x 10⁶ per in
Fig 12

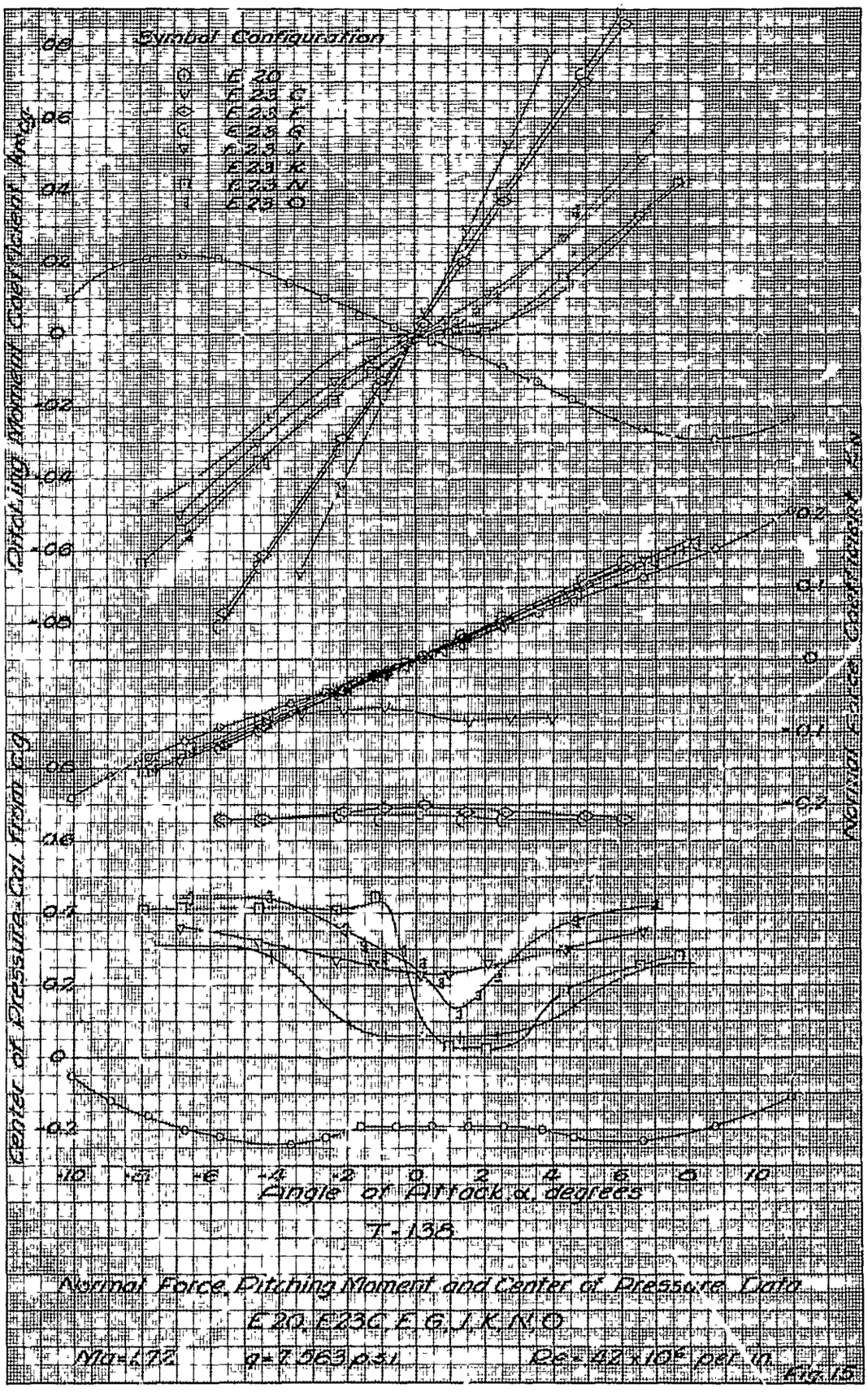
Symbol Configuration
E 20
E 23 C
E 23 E
E 23 G
E 23 J
E 23 K
E 23 N
E 23 O
Pitching Moment Coefficient, Cm
Normal Force Coefficient, CN
Center of Pressure Coef. Xcp/c.g.
Angle of Attack α, degrees
T-135
Normal Force, Pitching Moment and Center of Pressure Data
E 20, E 23C, E 6, J, K, N, O
Ma=1.72
q=7.563 psi
Re=4.2 x 10⁶ per ft.
Fig. 15

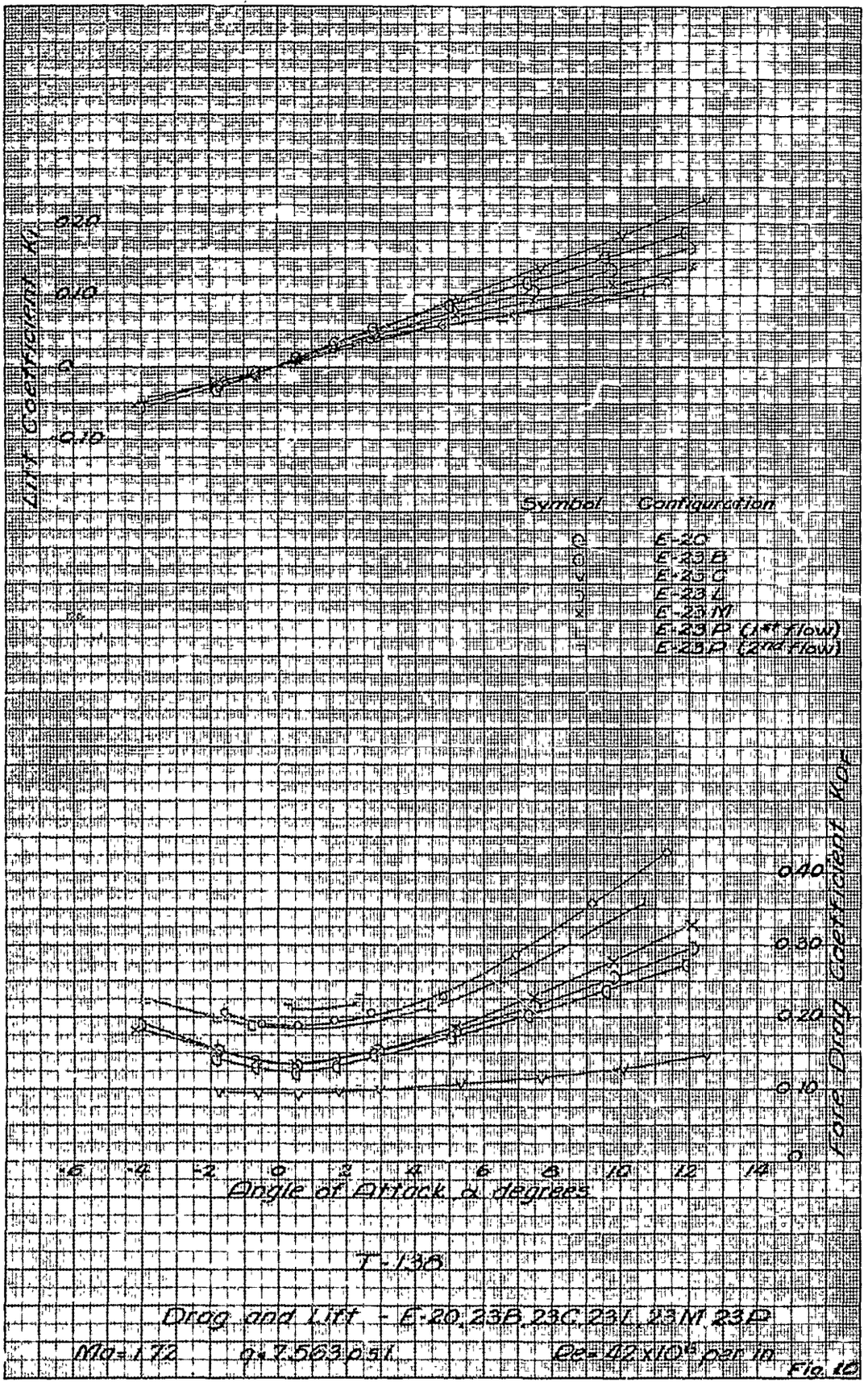
Lift Coefficient, C_L
0.20
0.40
0.10
Symbol
Configuration
E-20
E-23 B
E-23 C
E-23 L
E-23 M
E-23 P (1st Flow)
E-23 P (2nd Flow)
Form Drag Coefficient, $K_0 C_L^2$
0.40
0.30
0.20
0.10
0
-6
-4
-2
0
2
4
6
8
10
12
14
Angle of Attack, α degrees
T-136
Drag and Lift - E-20, 23B, 23C, 23L, 23M, 23P
Ma=1.72
q=7.563 psi
Re=.42x10⁶ per in
Fig. 10

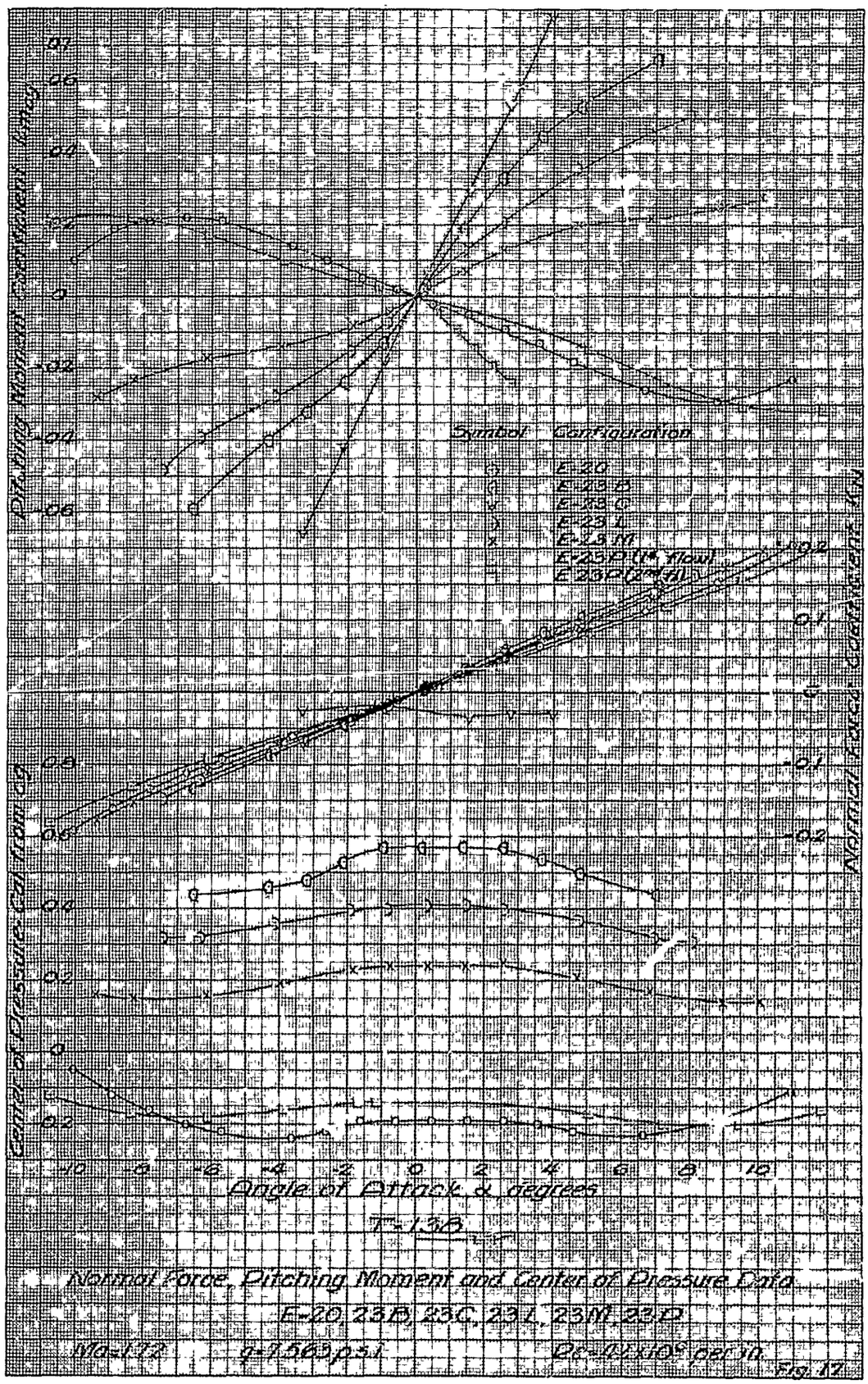
Pitching Moment Coefficient, C_m
Center of Pressure, fraction of body length from nose
Normal Force Coefficient, C_N
Symbol Configuration
E-20
E-23 B
E-23 C
E-23 L
E-23 M
E-23 P (1st flow)
E-23 P (2nd flow)
Angle of Attack, α, degrees
T-136
Normal Force, Pitching Moment and Center of Pressure Data
E-20, 23B, 23C, 23L, 23M, 23P
Ma=1.72 q=7.56 psi Re=0.5×10⁶ per in. Fig. 17

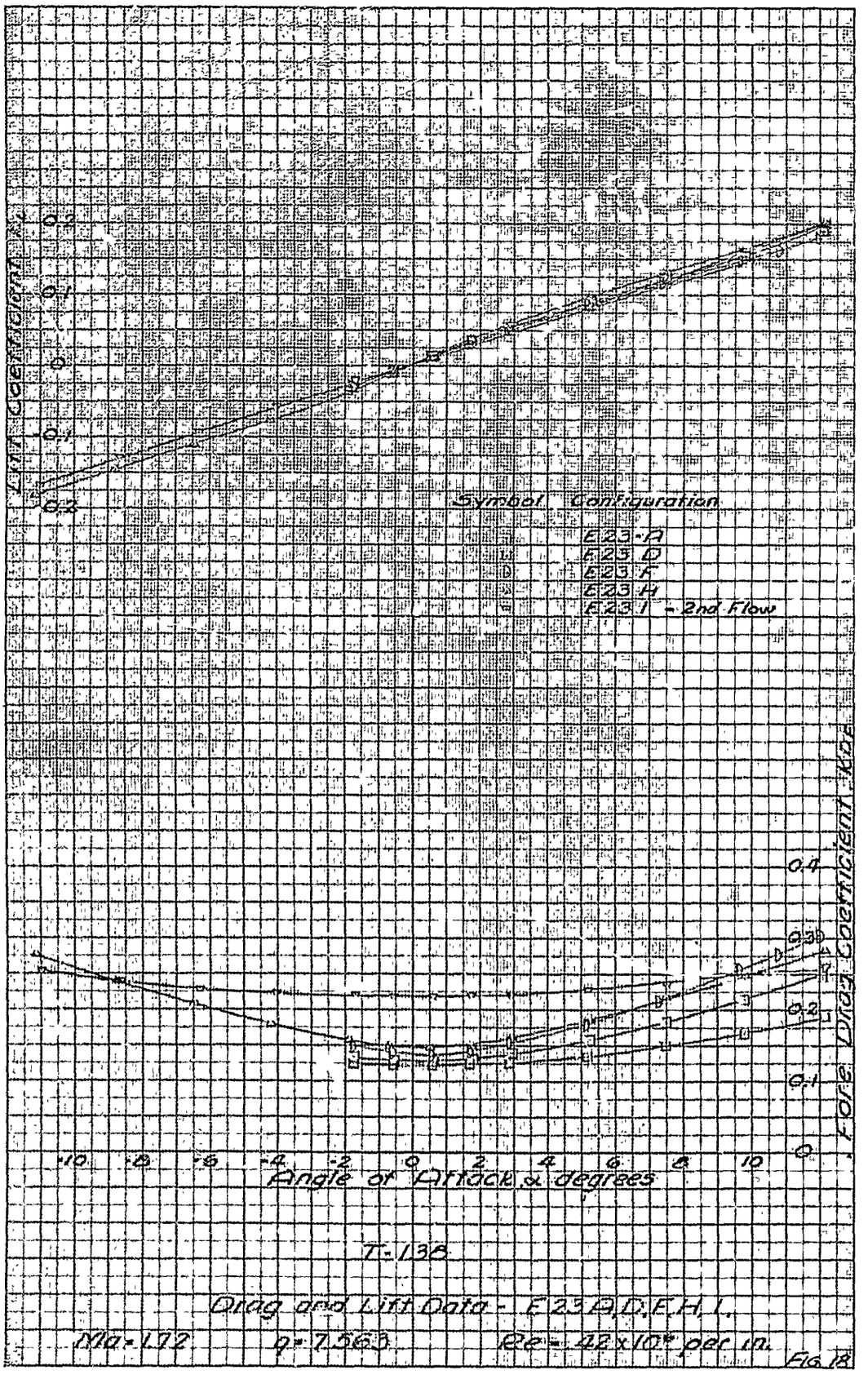
Lift Coefficient, C_L
Drag Coefficient, C_D
Symbol Configuration
E23-A
E23 D
E23 F
E23 H
E23 I - 2nd Flow
Angle of Attack, α degrees
-10
-8
-6
-4
-2
0
2
4
6
8
10
0.4
0.3
0.2
0.1
0
-0.1
-0.2
T-138
Drag and Lift Data - E23 A, D, F, H, I.
Nα = 1.72
q = 7.563
Re = .42 x 10⁶ per in.
Fig 18

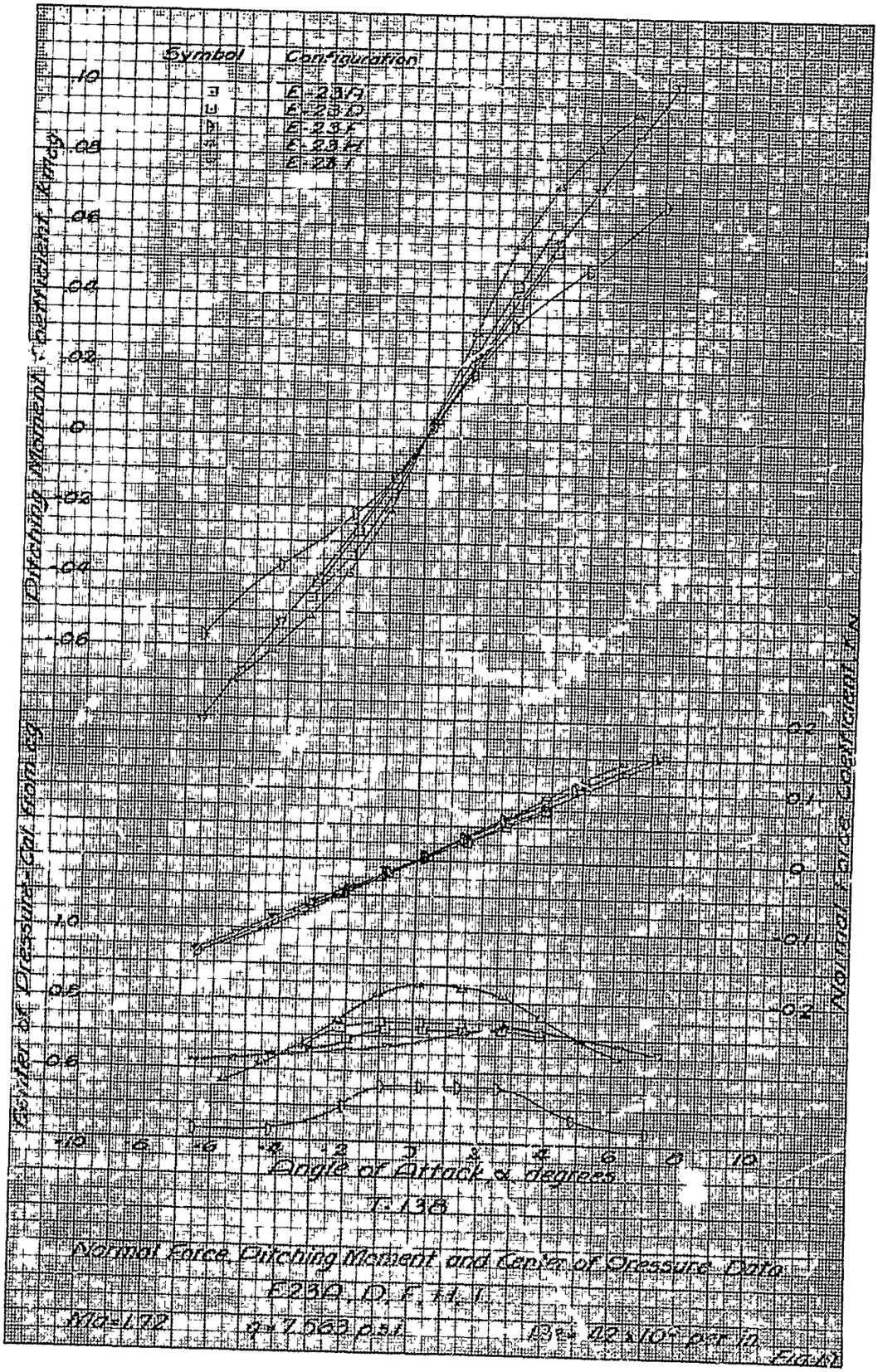
Symbol
Configuration
E-23(A)
E-23D
E-23F
E-23H
E-23I
Center of Pressure for Pitching Moment, Percent
Pitching Moment Coefficient, C_m
Normal Force Coefficient, C_N
Angle of Attack α, degrees
T-138
Normal Force, Pitching Moment and Center of Pressure Data
E23D, D, F, H, I
M_D=1.72
q=7,563 p.s.i.
R_e= 22 x 10⁶ per in.

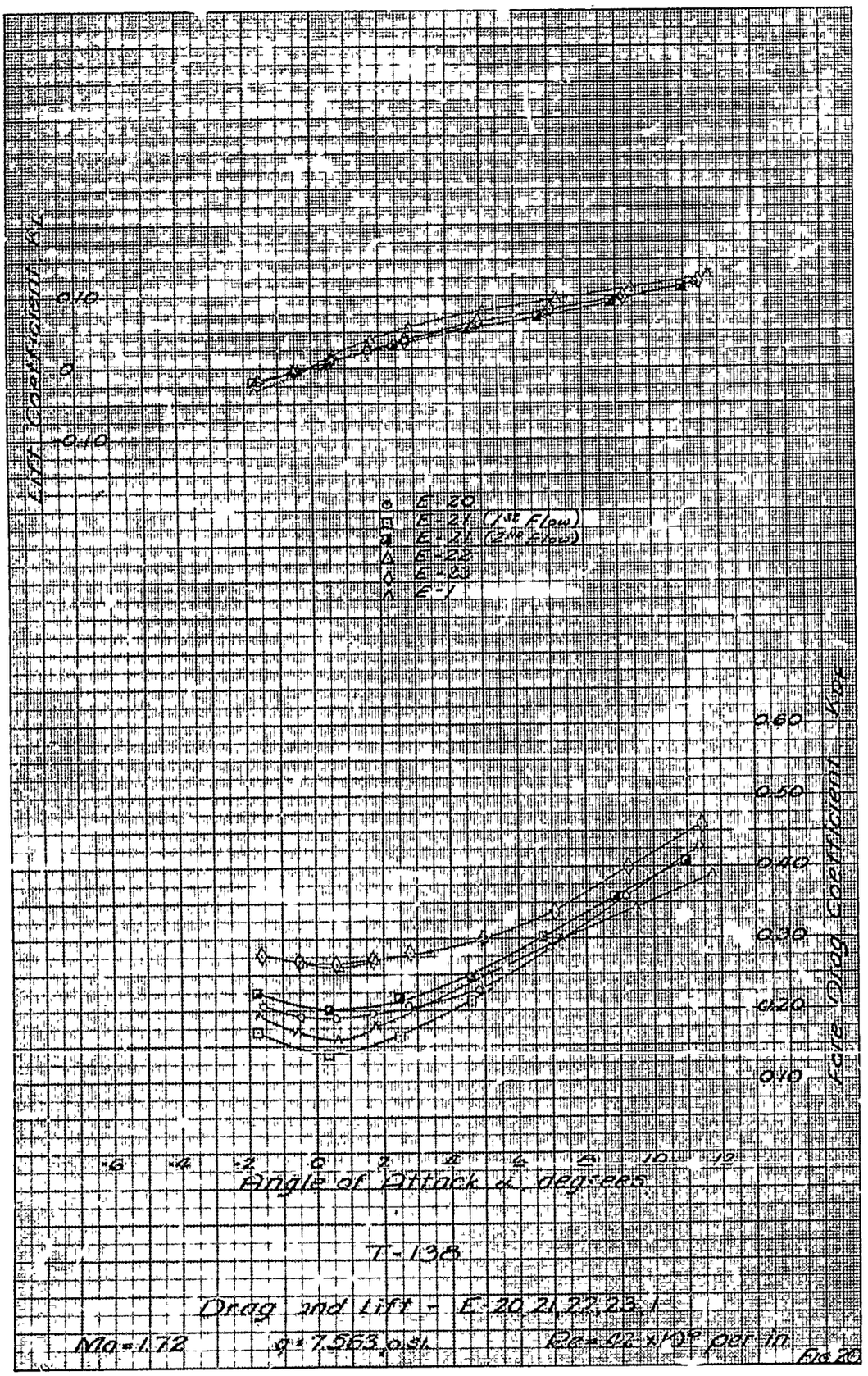
Lift coefficient C_L
0.10
0
-0.10
E-20
E-21 (1st Flow)
E-21 (2nd Flow)
E-22
E-23
E-1
0.60
0.50
0.40
0.30
0.20
0.10
Code Drag coefficient C_{DC}
-6
-4
-2
0
2
4
6
8
10
12
Angle of Attack α, degrees
T-138
Drag and Lift - E-20 21, 22, 23, 1
Mo = 1.72
q = 7,563 p.s.f.
Re = 42 x 10⁶ per in.
Fig 20

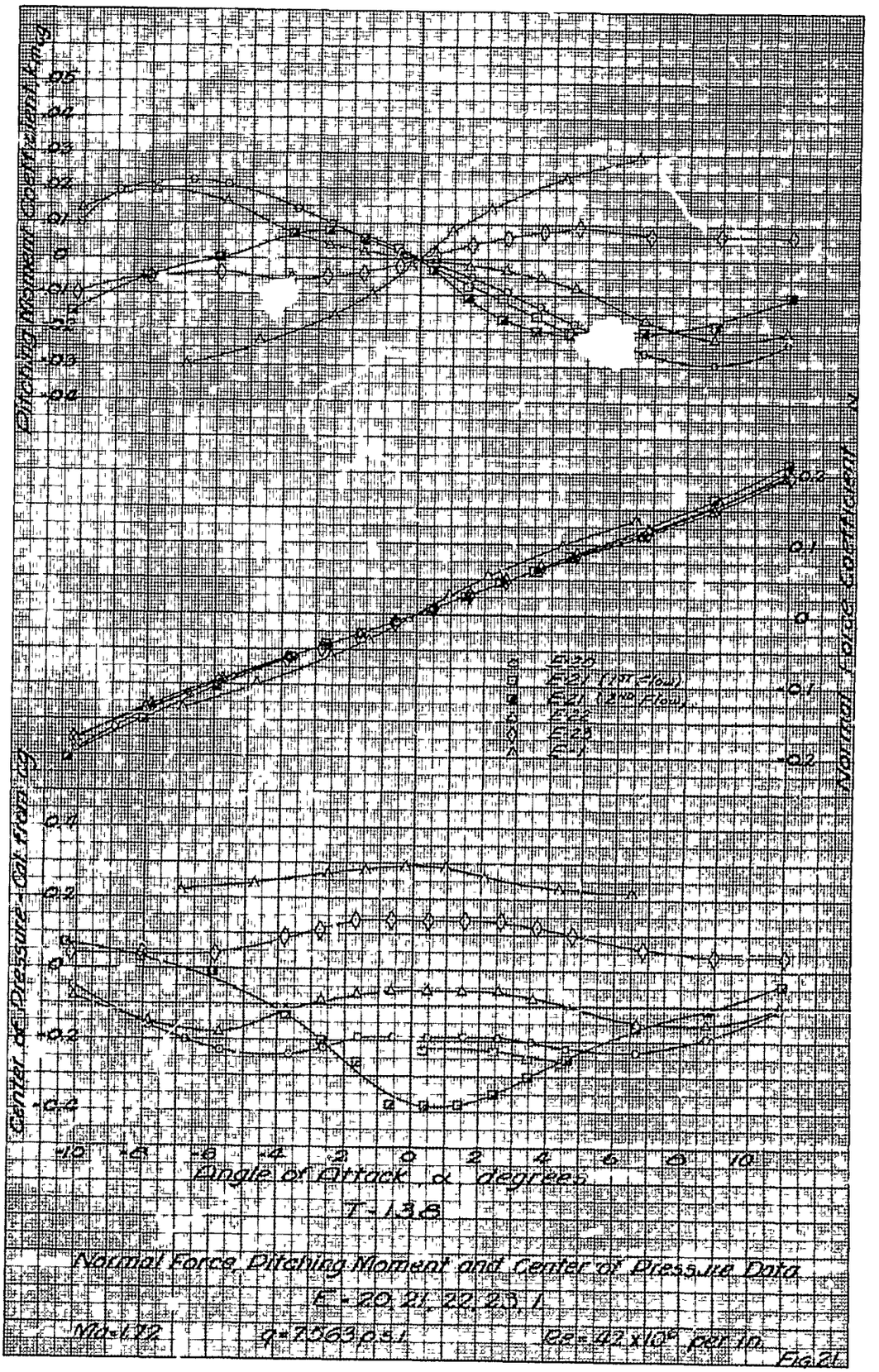

T-138

Normal Force, Pitching Moment and Center of Pressure Data

E-20, 21, 22, 23, 1

M_d=1.72 q=7563.0 s.f. C_e=.42 x 10^{-6} per in. Fig 21

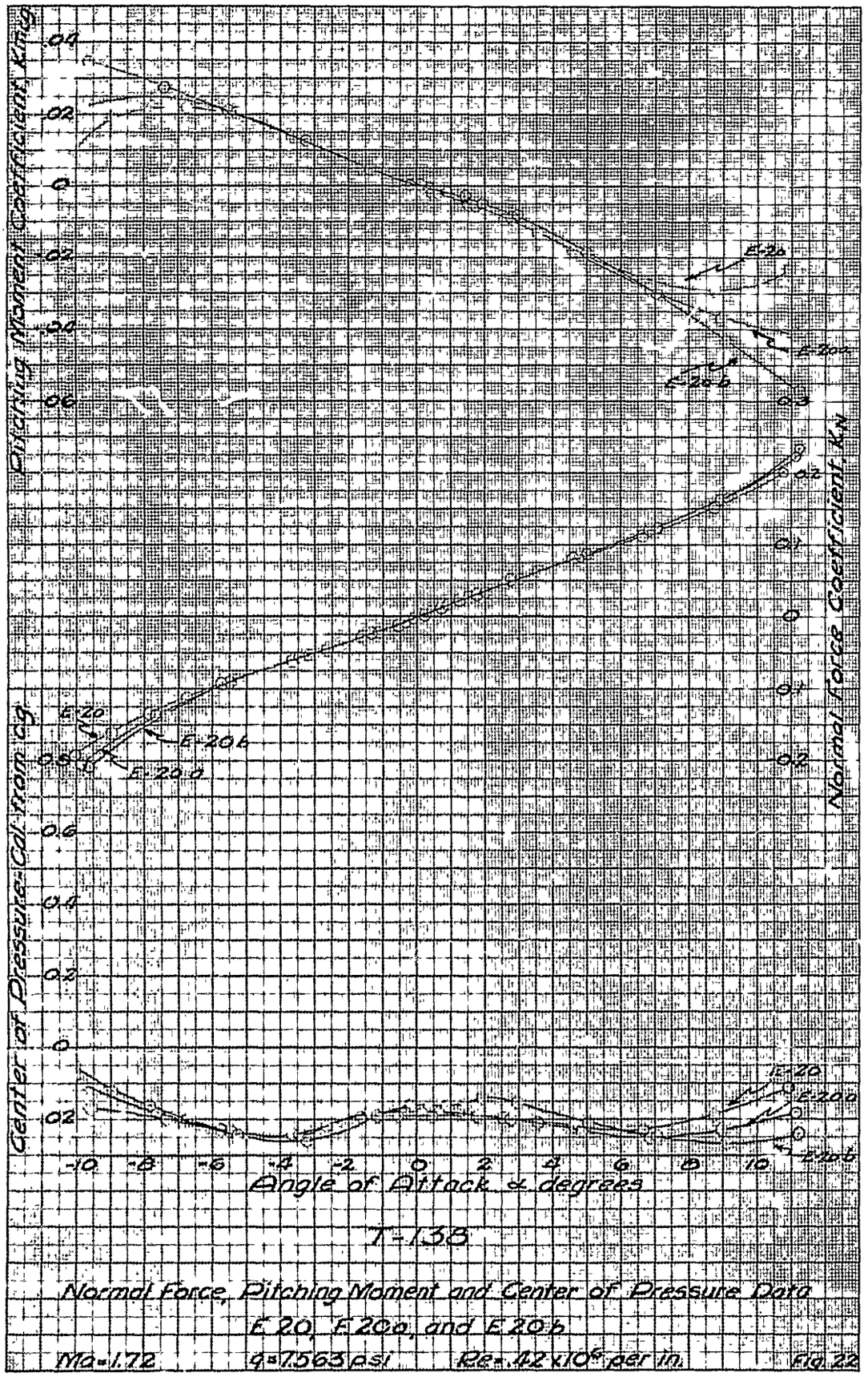

T-138

Normal Force, Pitching Moment and Center of Pressure Data

E 20, E 20a, and E 20b

Ma-1.72 q=1563 psi Re=.42 x10^6 per in. Fig 22

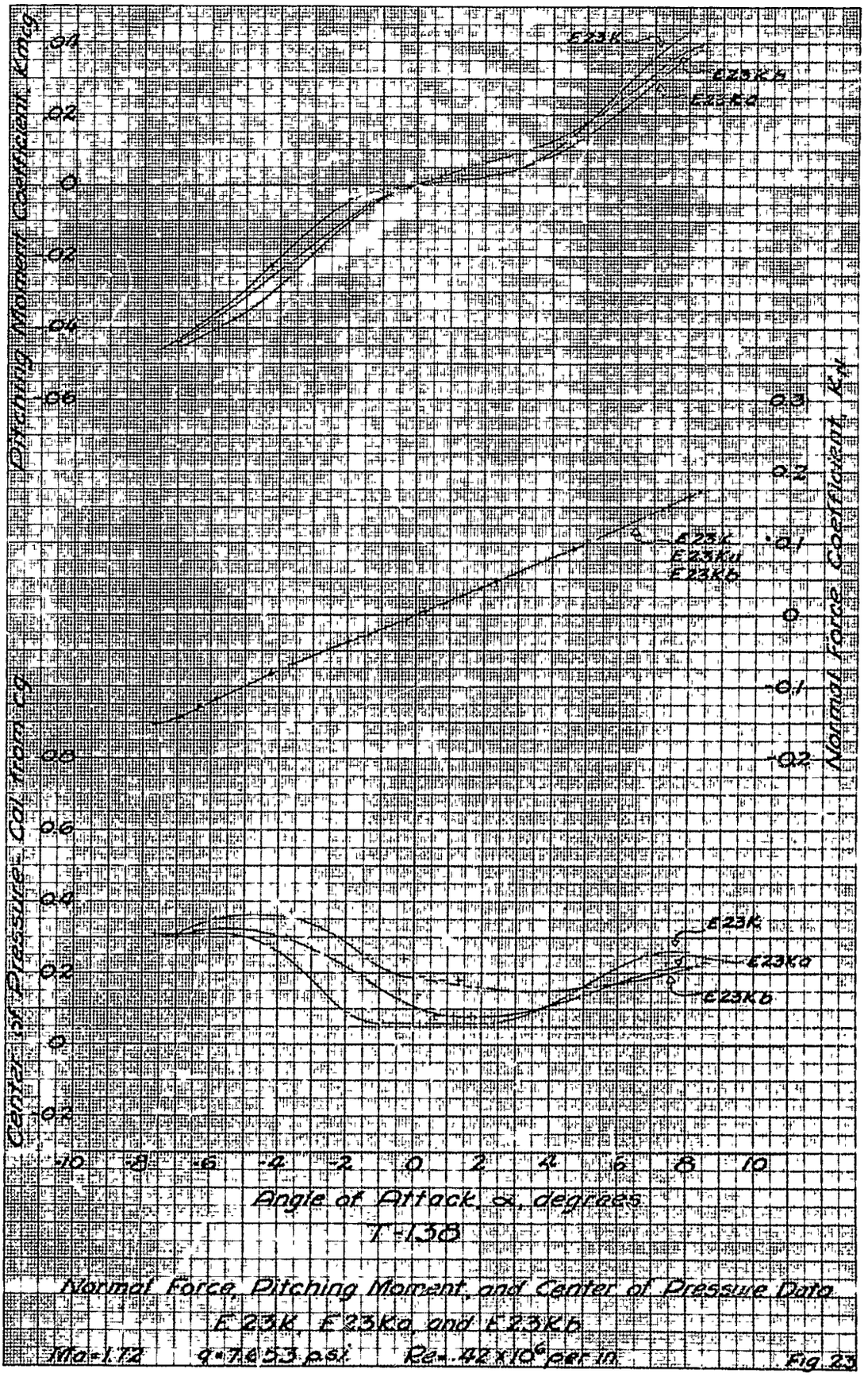

Normal Force, Pitching Moment, and Center of Pressure Data
E 23K, E 23Ka, and E 23Kb
M_a=1.72 q=7653 psi R_e=.42×10^6 per in. Fig 23

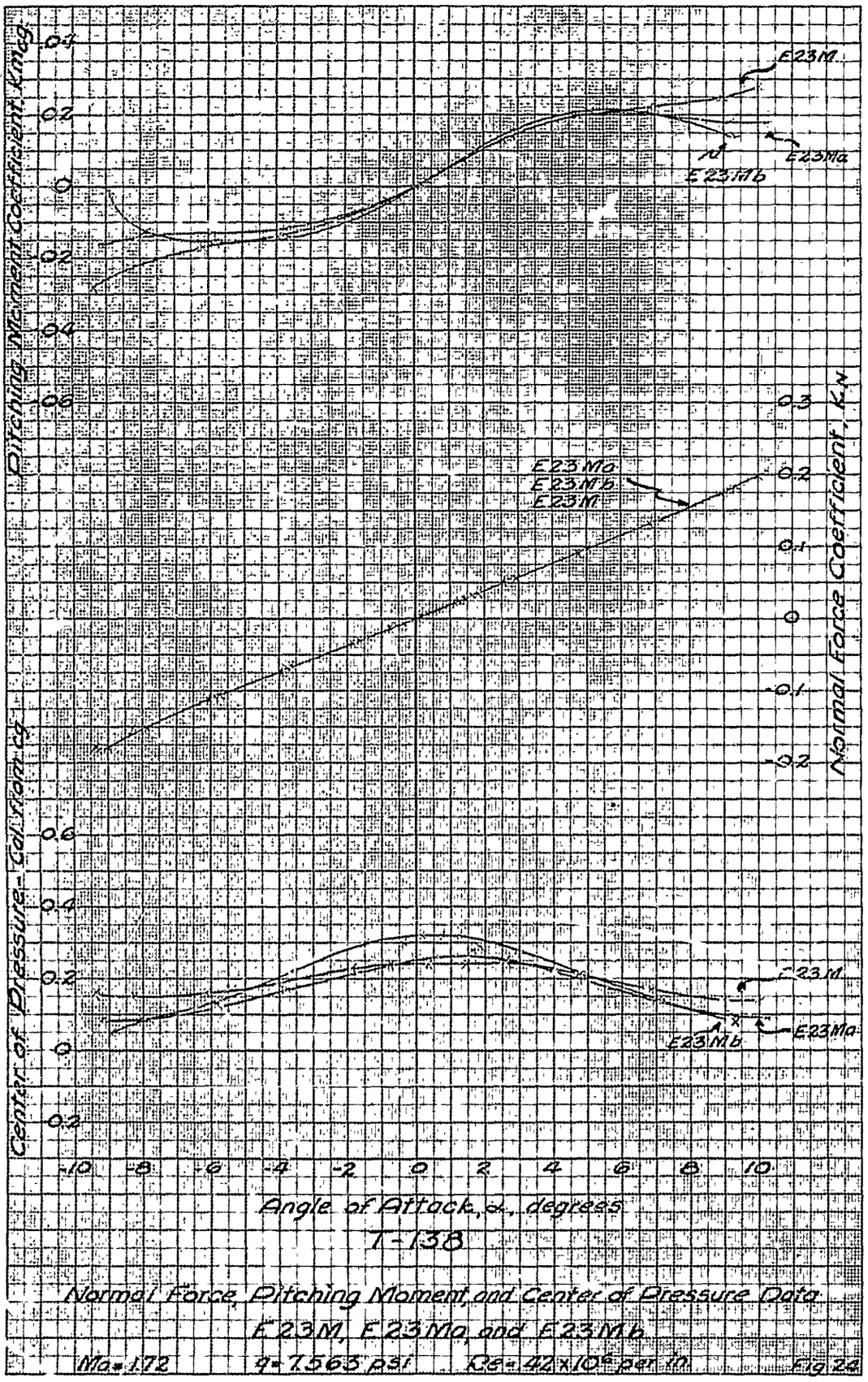

T-138

Normal Force, Pitching Moment, and Center of Pressure Data
E23M, E23Ma, and E23Mb

M_a = 1.72 q = 7565 psi R_e = 42 x 10^6 per in. Fig 24

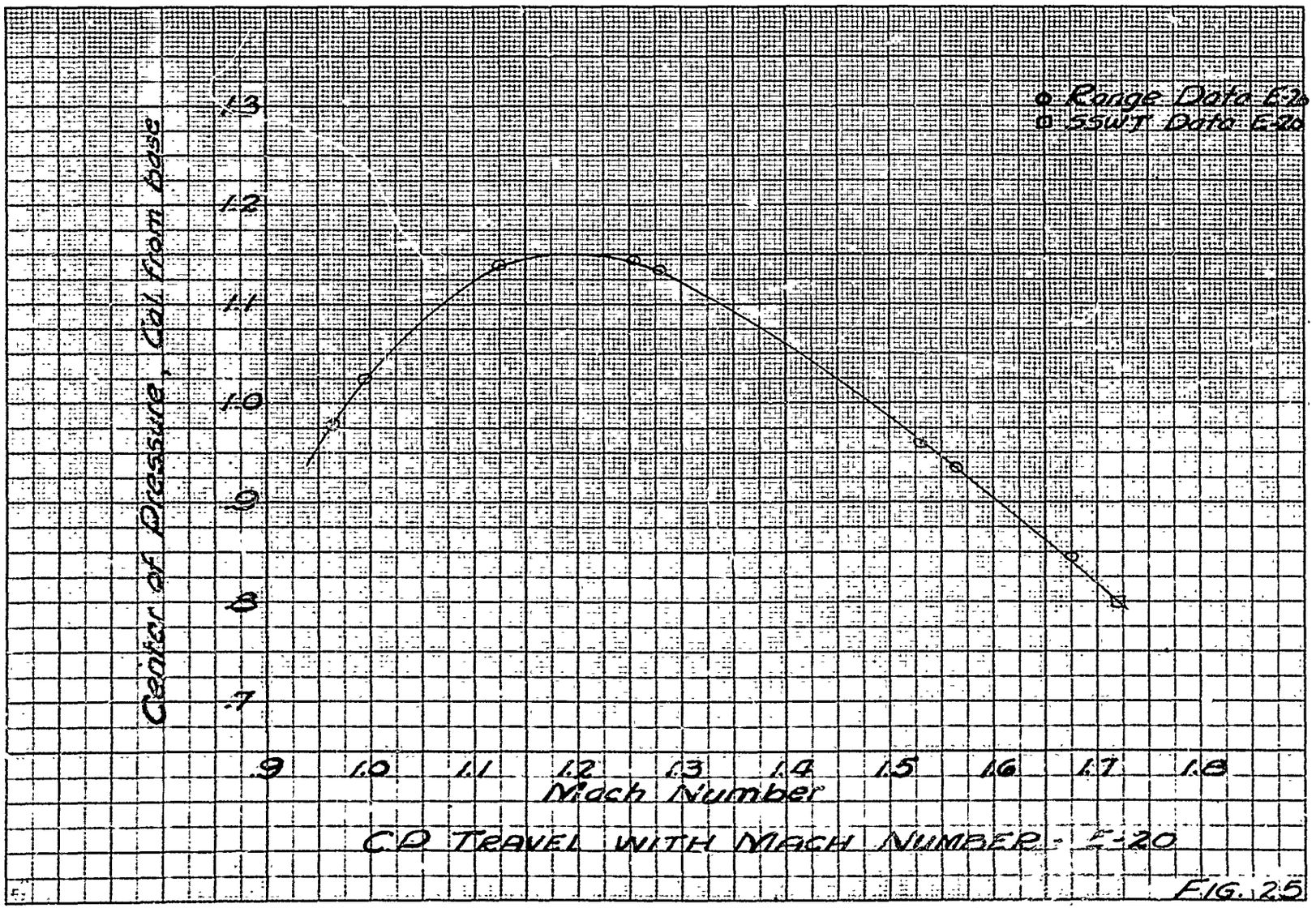

C.P. TRAVEL WITH MACH NUMBER - E-20

FIG. 25

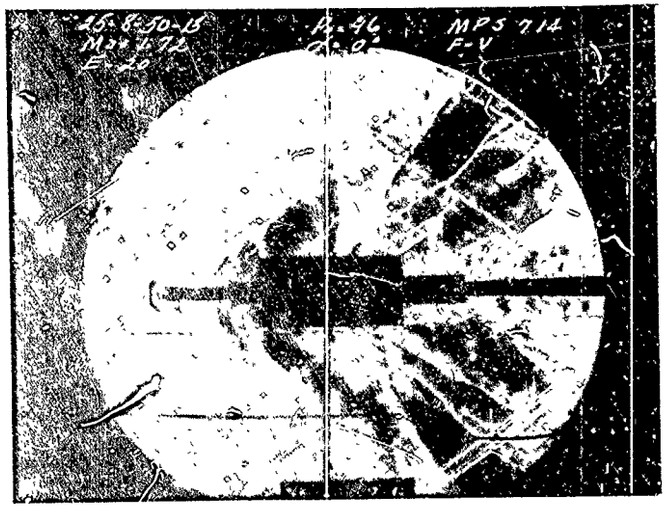

FIG. 26 B 236 - Schlieren Picture of E-20 - $\alpha = 0$

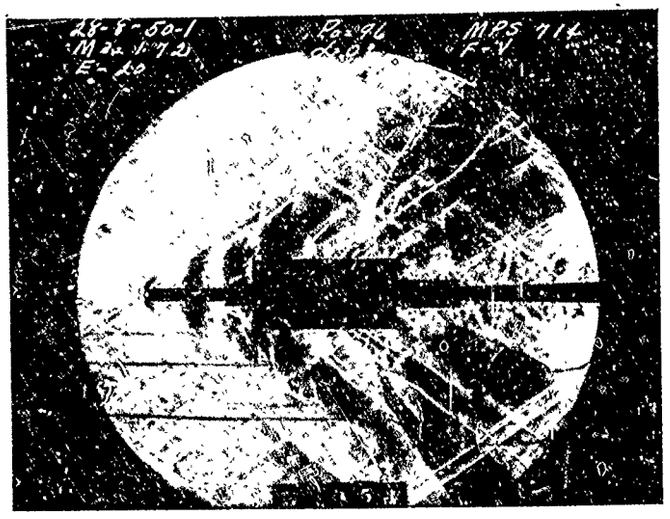

FIG. 27. B 254 - Schlieren Picture of E-20 - $\alpha = 0$

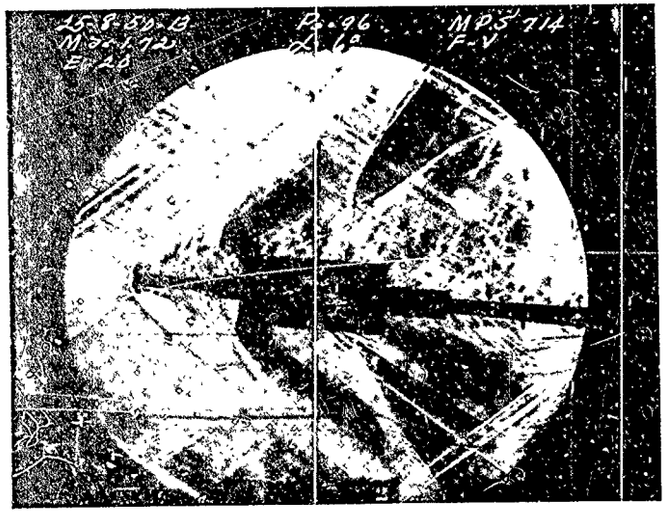

FIG 28. B 242 - Schlieren Picture of E-20 - $\alpha = 6$

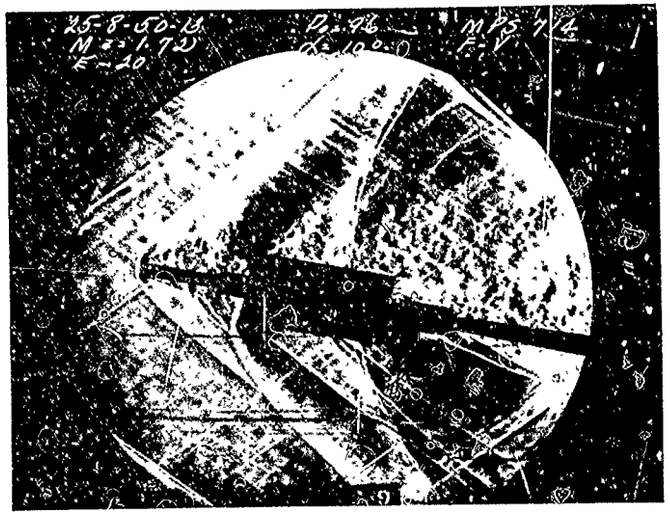

FIG. 29. B 239 - Schlieren Picture of E-20 - $\alpha = 10$

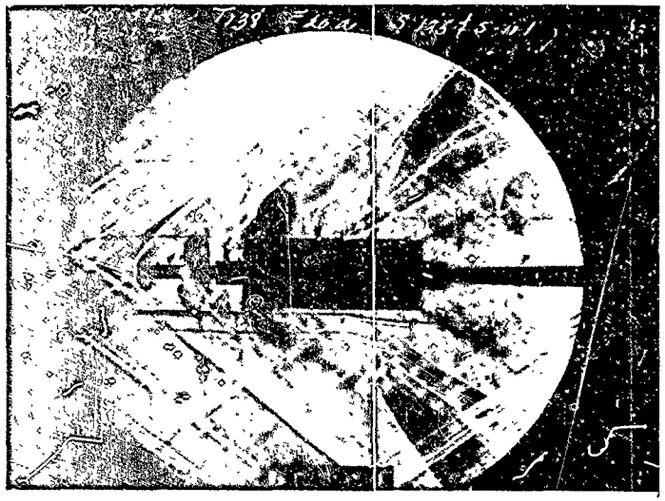

FIG 30 B 1700 - Schlieren Picture of E-20a - $\alpha = 0$

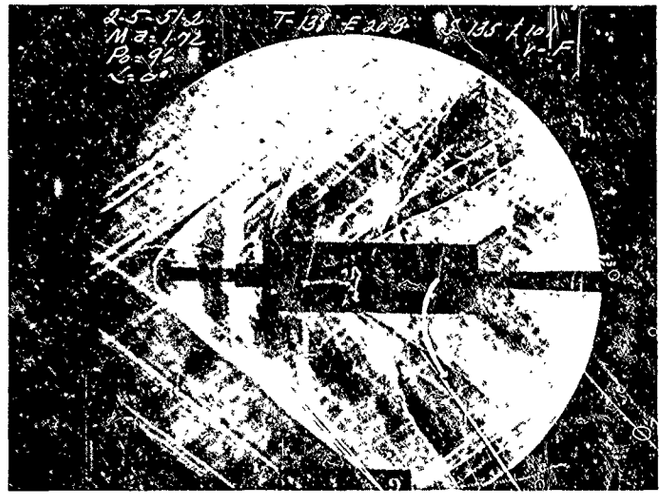

FIG. 31. B 1709 - Schlieren Picture of E-20b - $\alpha = 0$

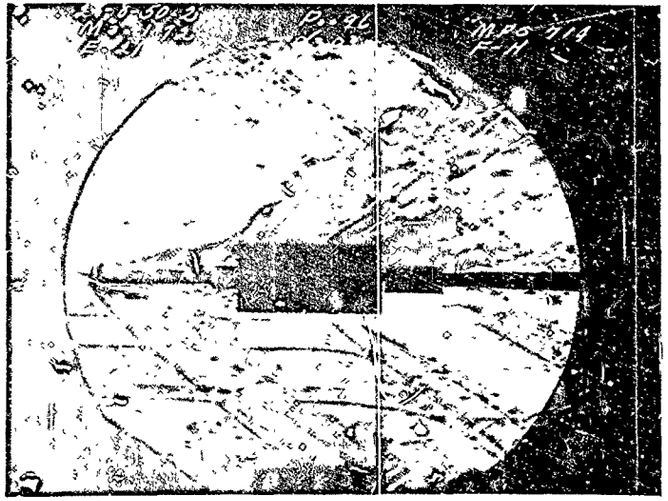

FIG. 32 B 258 - Schlieren Picture of E- 21 - $\alpha = 0$
First Flow Pattern

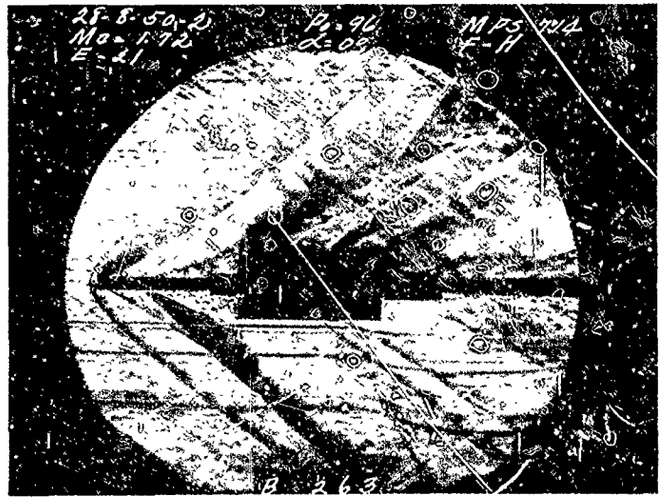

FIG. 33. B 263 - Schlieren Picture of E-21 - $\alpha = 0$
Second Flow Pattern

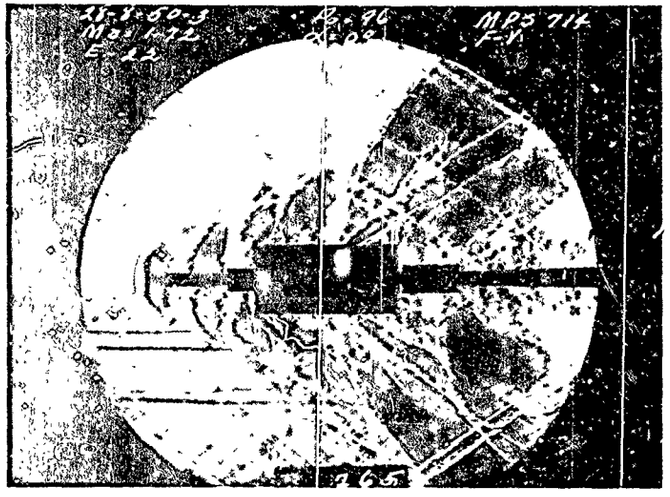

FIG. 34. B 265 - Schlieren Picture of E-22 - $\alpha = 0$

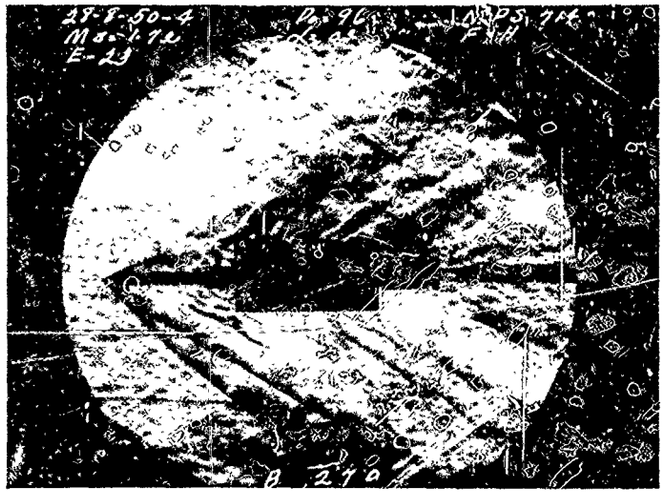

FIG. 35. B 270 - Schlieren Picture of E-23 - $\alpha = 0$

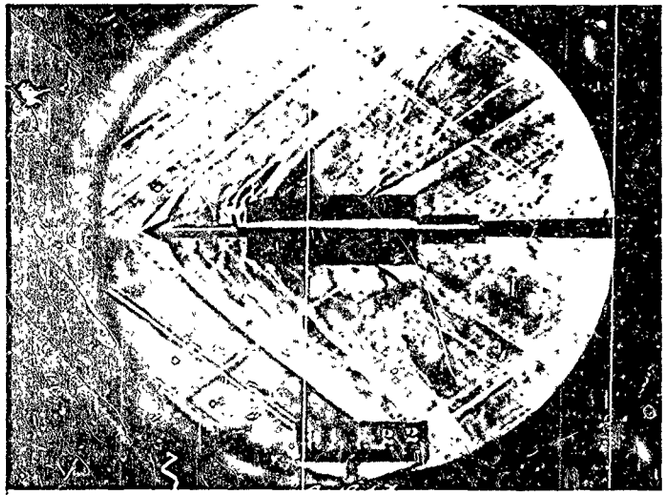

FIG. 36. B 1822 - Schlieren Picture of E-23A - $\alpha = 0$

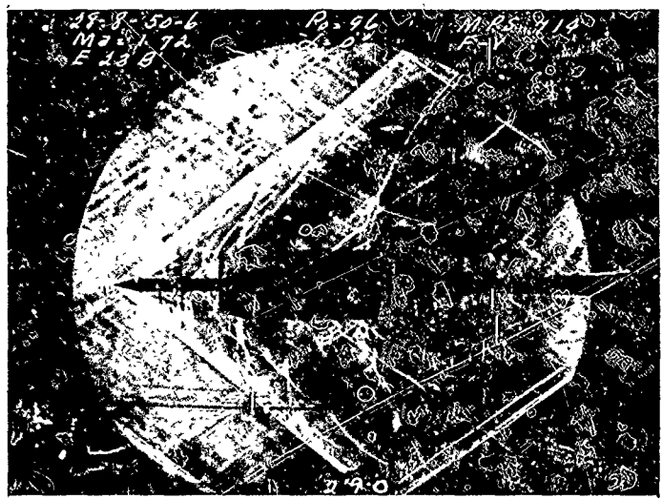

FIG. 37. B 290 - Schlieren Picture of E-23B - $\alpha = 0$

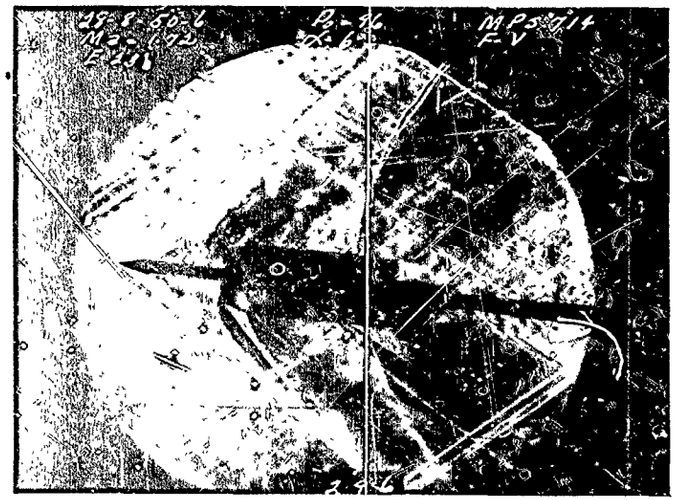

FIG. 38 B 296 - Schlieren Picture of E-23B - $\alpha = 6$

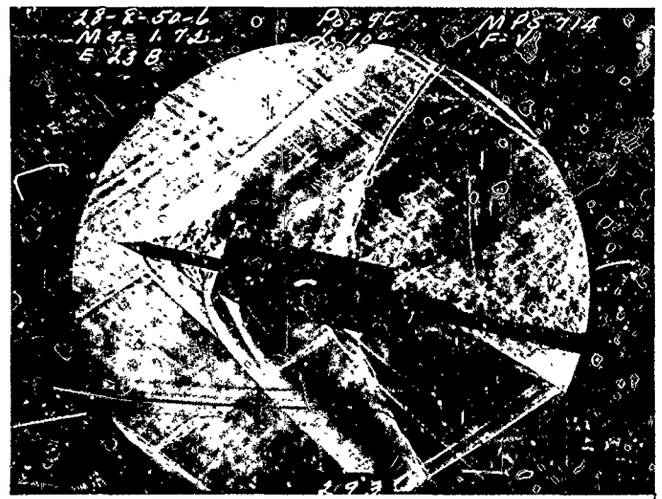

FIG. 39. B 293 - Schlieren Picture of E-23B - $\alpha = 10$

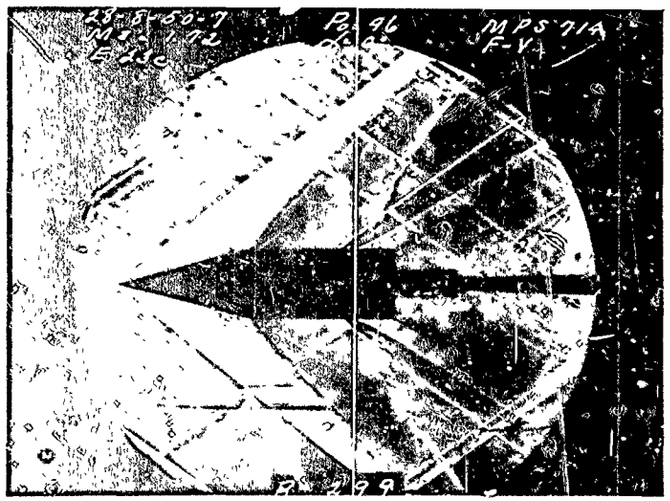

FIG. 40. B 299 - Schlieren Picture of E-23C - $\alpha = 0$

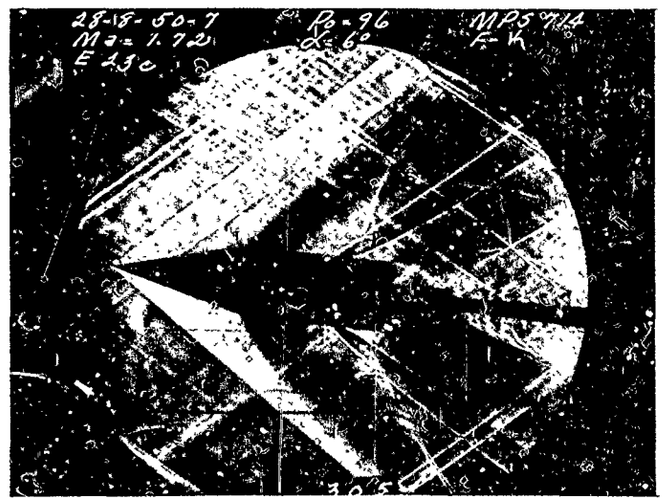

FIG. 41. B 305 - Schlieren Picture of E-23C - $\alpha = 6$

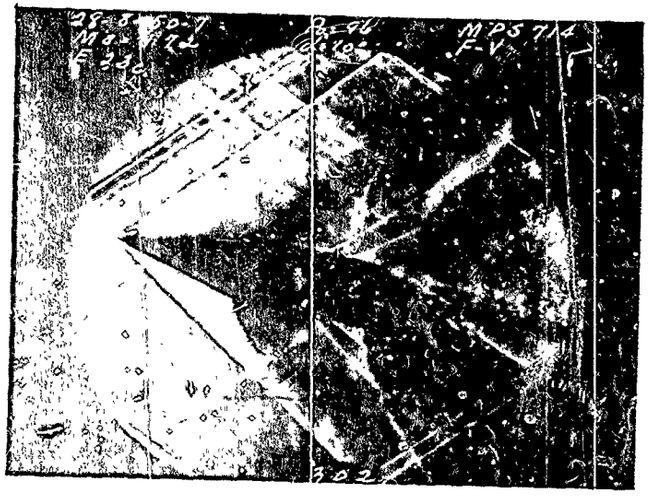

FIG. 42. B 302 - Schlieren Picture of E-23C - $\alpha = 10$

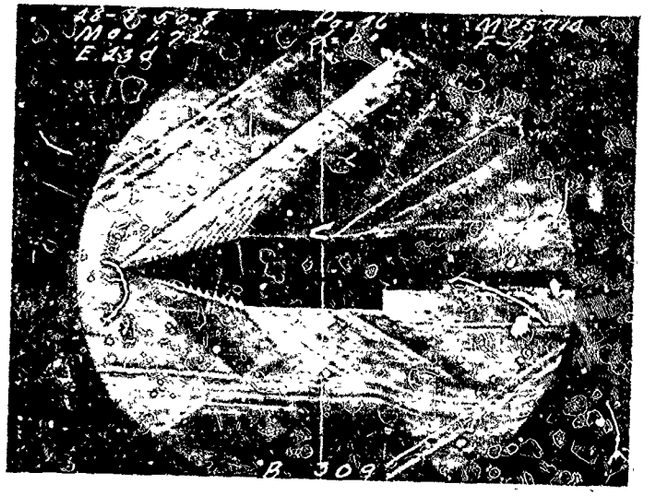

FIG. 43. B 309 - Schlieren Picture of E-23D - $\alpha = 0$

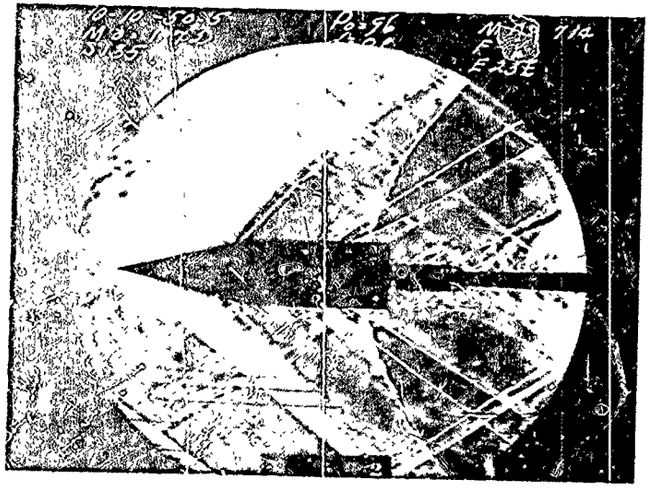

FIG. 44. B 502 - Schlieren Picture of E-23E - $\alpha = 0$
20 x 20 mesh, 56% solidity

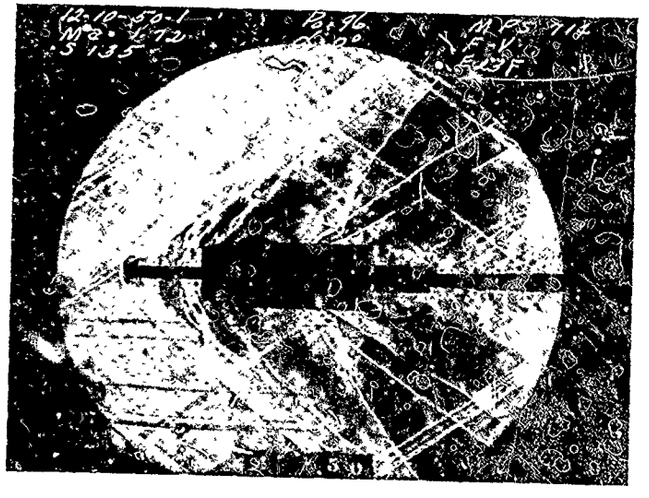

FIG. 45. B 550 - Schlieren Picture of E-23F - $\alpha = 0$

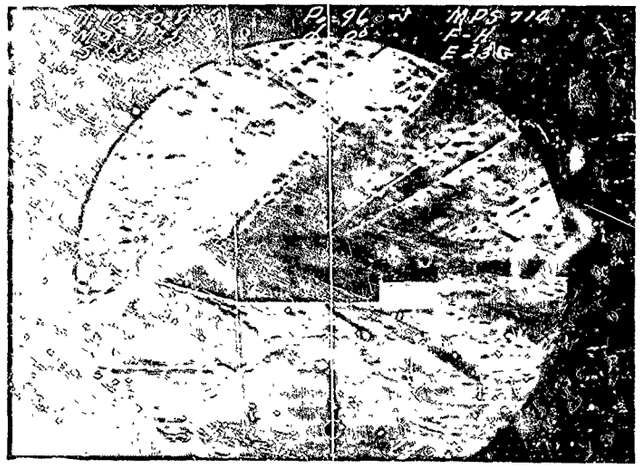

FIG. 46. B 532 - Schlieren Picture of E-23G - $\alpha = 0$
20 x 20 mesh, 36% solidity

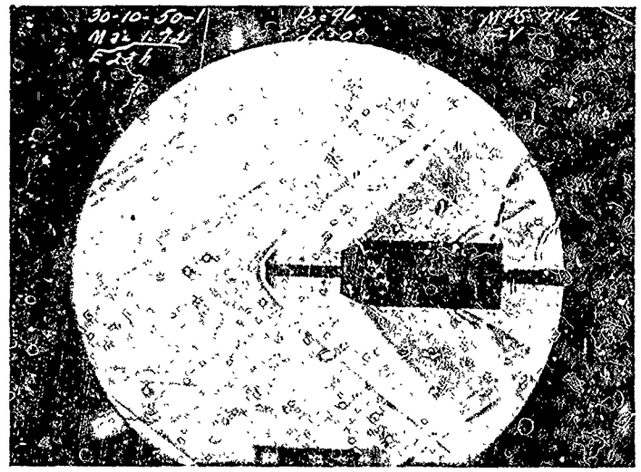

FIG. 47. B 653 - Schlieren Picture of E-23H - $\alpha = 0$

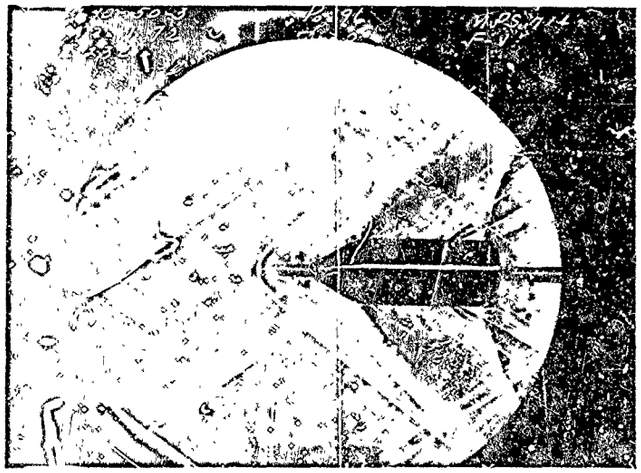

FIG. 48. B 644 - Schlieren Picture of E-23I - $\alpha = 0$
First Flow Pattern

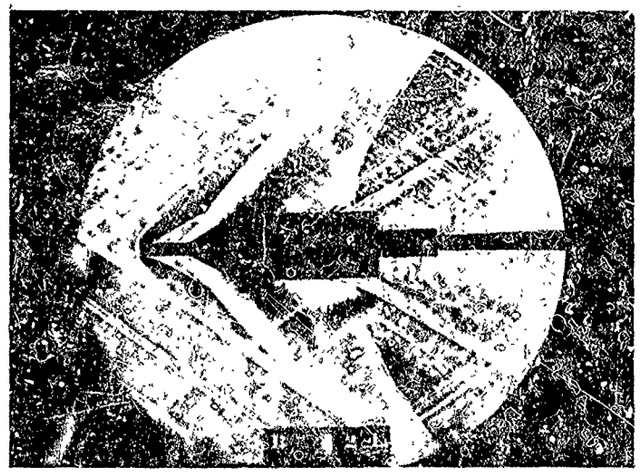

FIG. 49. B 1824 - Schlieren Picture of E-23I - $\alpha = 0$
Second Flow Pattern

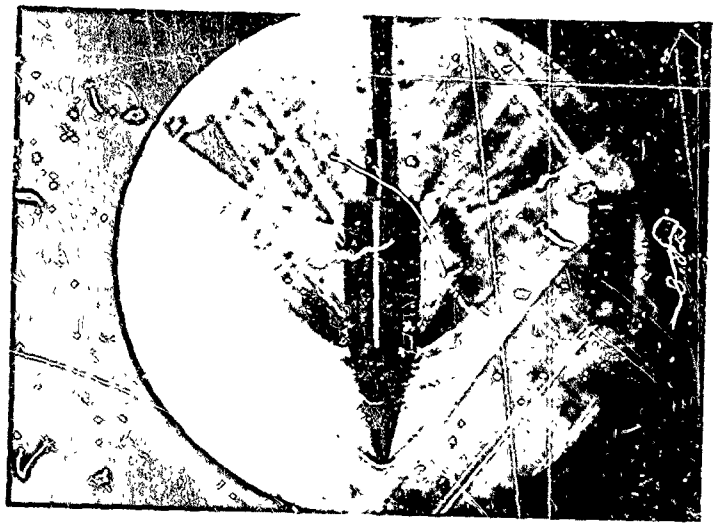

FIG. 50. B 1825 - Schlieren Picture of E-23J - $\alpha = 0$
20 x 20 mesh, 56% solidity

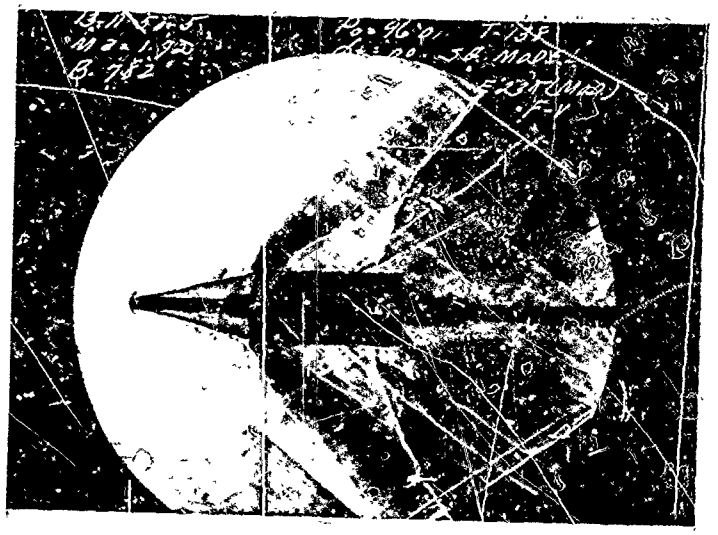

FIG. 51. B 782 - Schlieren Picture of E-23K - $\alpha = 0$
13 x 18 mesh, 31% solidity

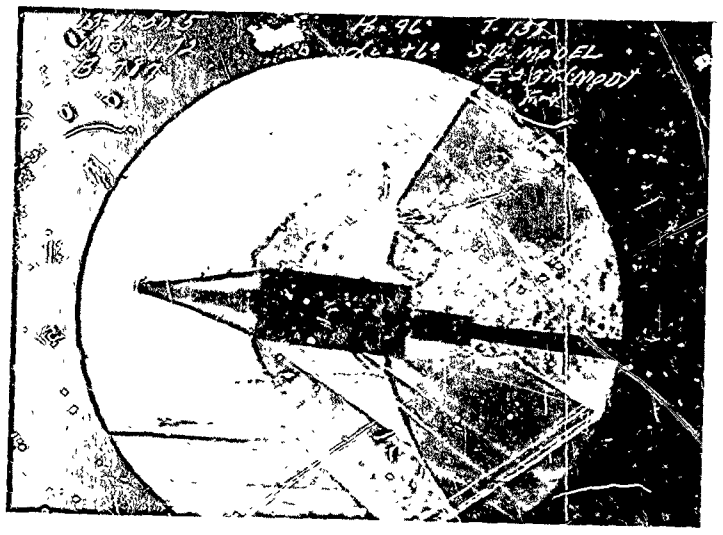

FIG. 52. B 787 - Schlieren Picture of E-23K - $\alpha = 6$
13 x 18 mesh, 31% solidity

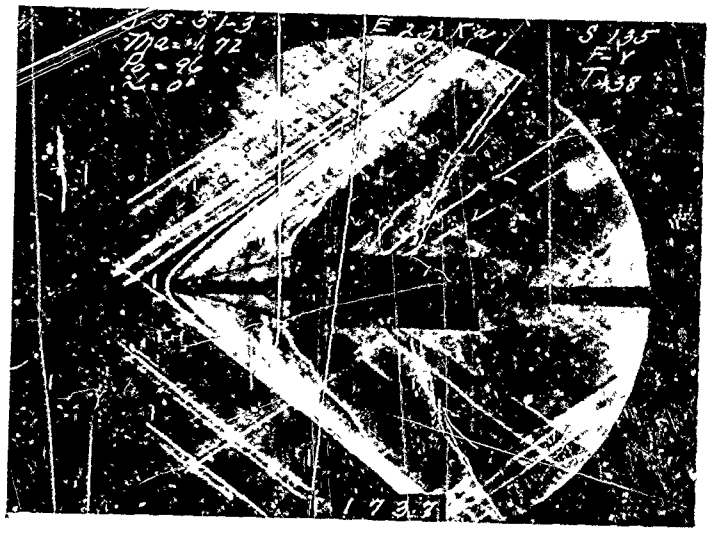

FIG. 53. B 1737 - Schlieren Picture of E-23Ka - $\alpha = 0$
13 x 18 mesh, 31% solidity

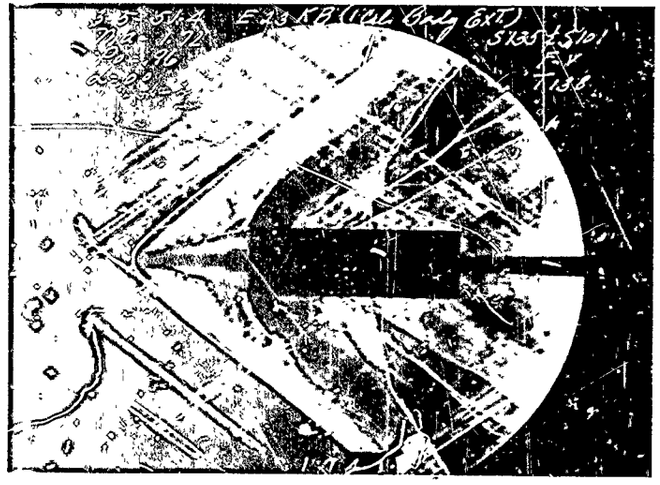

FIG. 54. B 1741 - Schlieren Picture of E-23KB - $\alpha = 0$
13 x 18 mesh, 31% solidity

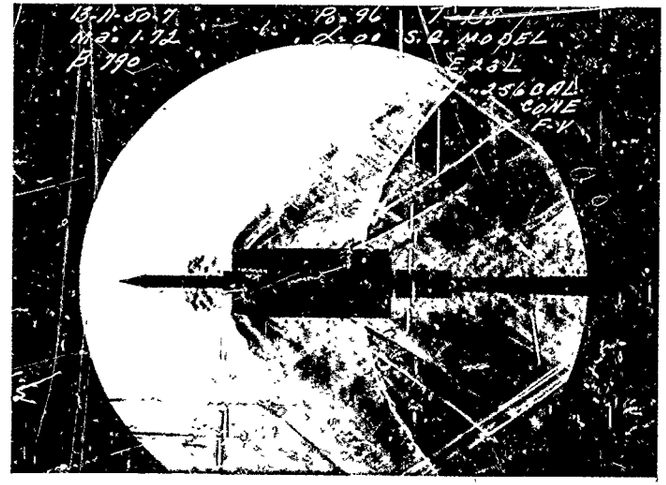

FIG. 55. B 790 - Schlieren Picture of E-23L - $\alpha = 0$

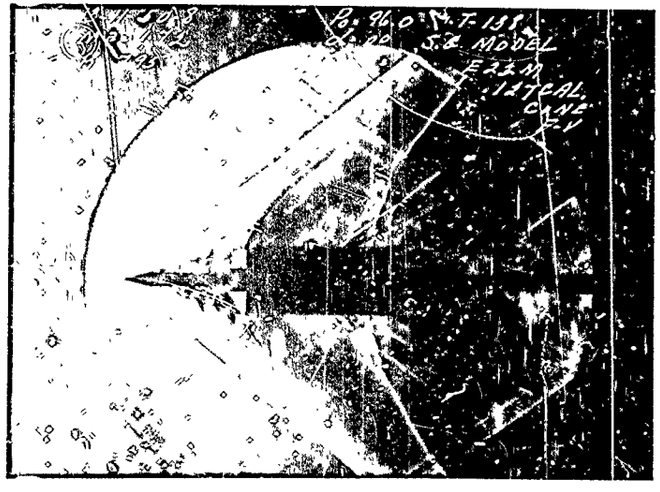

FIG. 56. B 794 - Schlieren Picture of E-23L - $\alpha = 6$

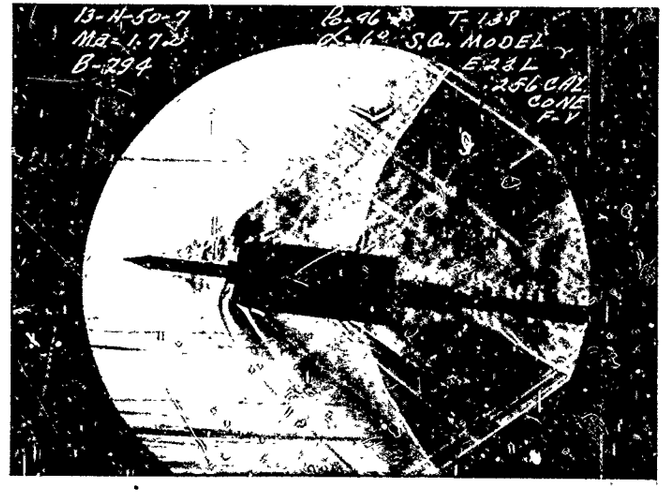

FIG. 57. B 795 - Schlieren Picture of E-23M - $\alpha = 0$

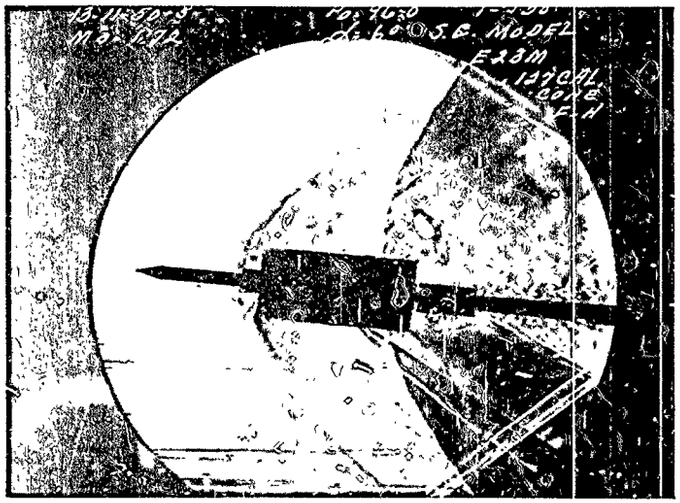

FIG. 58. B 799 - Schlieren Picture of E-23M - $\alpha = 6$

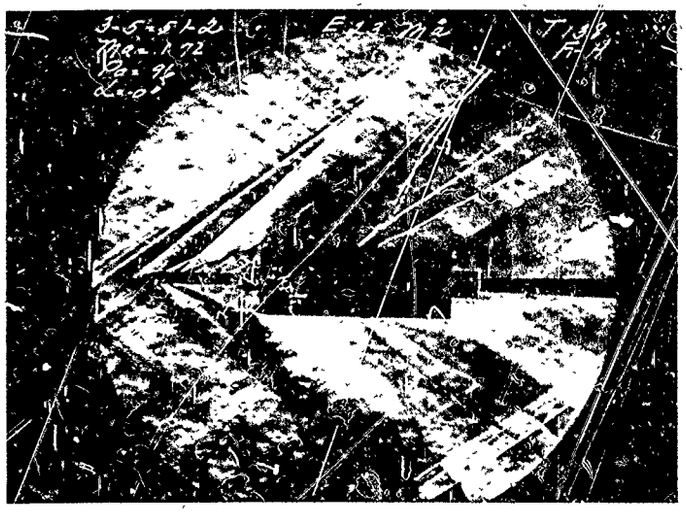

FIG. 59. B 1731 - Schlieren Picture of E-23Ma - $\alpha = 0$

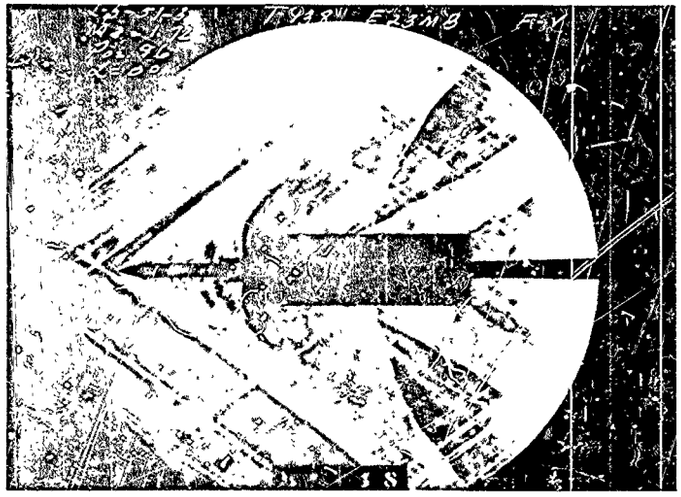

FIG. 60. B 1718 - Schlieren Picture of E-23MB - $\alpha = 0$

FIG. 61. B 822 - Schlieren Picture of E-23N - $\alpha = 0$
4 x 4 mesh, 19% solidity

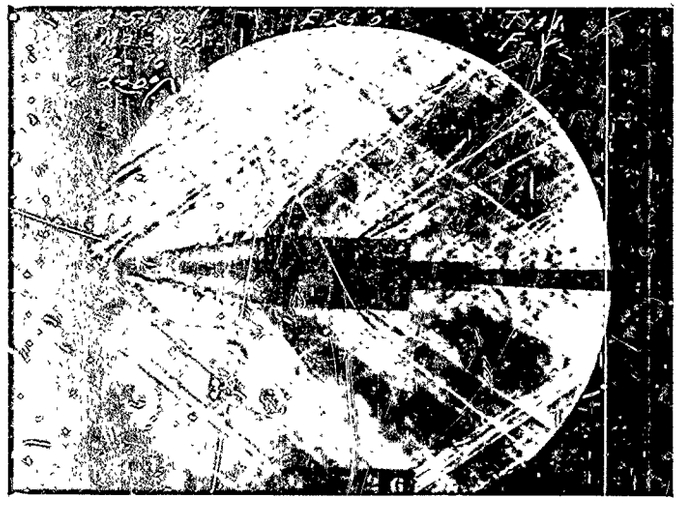

FIG. 62. B 1726 - Schlieren Picture of E-23"0" - $\alpha = 0$
13 x 18 mesh, 31% solidity

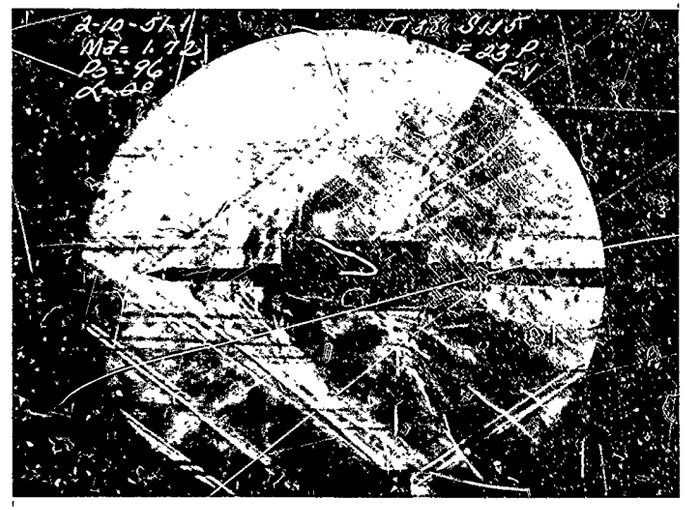

FIG, 63. B 1991 - Schlieren Picture of E-23P - $\alpha = 0$
First Flow Pattern

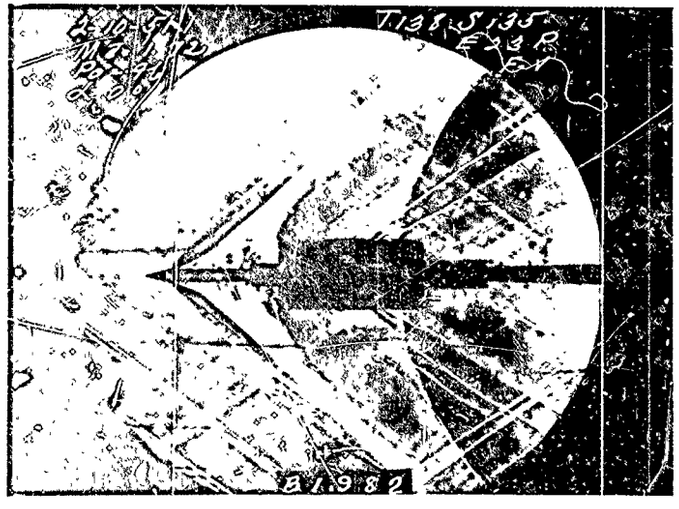

FIG. 64. B 1982 - Schlieren Picture of E-23P - $\alpha = 0$
Second Flow Pattern

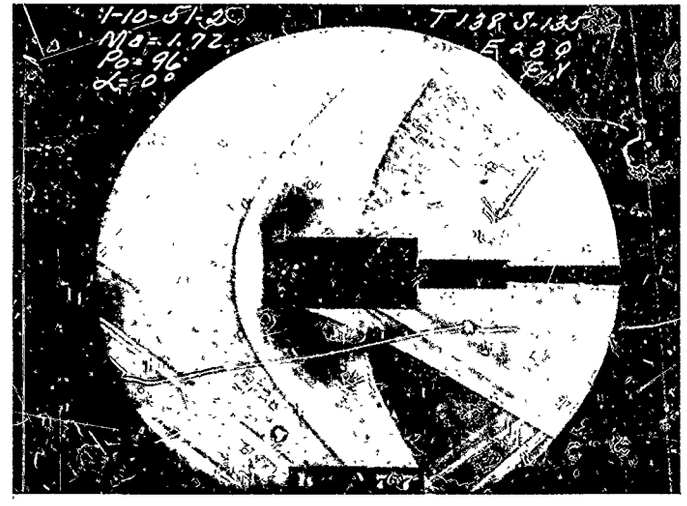

FIG. 65. B 1977 - Schlieren Picture of E-23Q - $\alpha = 0$

FIG. 66. B 539 - Schlieren Picture of E-1 - $\alpha = 0$

ARMY---OS---ABERDEEN PROVING GROUND, MD-- 1174